Research article

JGS
Journal of the Geological Society

Published Online First

https://doi.org/10.1144/jgs2021-066

New onshore insights into the role of structural inheritance during Mesozoic opening of the Inner Moray Firth Basin, Scotland

Alexandra Tamas[1*], Robert E. Holdsworth[1,2], John R. Underhill[3], Dan M. Tamas[4], Edward D. Dempsey[5], Kit Hardman[5], Anna Bird[5], Dave McCarthy[6], Ken J.W. McCaffrey[1,2] and David Selby[1,7]

[1] Department of Earth Sciences, Durham University, Durham DH1 3LE, UK
[2] Geospatial Research Ltd, Durham DH1 4EL, UK
[3] Shell Centre for Exploration Geoscience, Institute of GeoEnergy Engineering, Heriot-Watt University, Edinburgh EH14 4AS, UK
[4] Centre for Integrated Geological Studies, Babes-Bolyai University, Cluj-Napoca, Romania
[5] Department of Geology, Hull University, Hull HU6 7RX, UK
[6] British Geological Survey, Edinburgh EH14 4AP, UK
[7] State Key Laboratory of Geological Processes and Mineral Resources, School of Earth Resources, China University of Geosciences, Wuhan, Hubei Province 430074, China

AT, 0000-0001-8010-1853; DMT, 0000-0002-6640-8928; EDD, 0000-0002-8425-2226; AB, 0000-0002-2496-4344; DM, 0000-0002-0677-773X

* Correspondence: alexandra.tamas@durham.ac.uk; tamas.alexandraaa@gmail.com

Abstract: The Inner Moray Firth Basin (IMFB) forms the western arm of the North Sea trilete rift system that initiated mainly during the Late Jurassic–Early Cretaceous with the widespread development of major NE–SW-trending dip-slip growth faults. The IMFB is superimposed over the southern part of the older Devonian Orcadian Basin. The potential influence of older rift-related faults on the kinematics of later Mesozoic basin opening has received little attention, partly owing to the poor resolution of offshore seismic reflection data at depth. New field observations augmented by drone photography and photogrammetry, coupled with U–Pb geochronology, have been used to explore the kinematic history of faulting in onshore exposures along the southern IMFB margin. Dip-slip north–south- to NNE–SSW-striking Devonian growth faults are recognized that have undergone later dextral reactivation during NNW–SSE extension. The U–Pb calcite dating of a sample from the synkinematic calcite veins associated with this later episode shows that the age of fault reactivation is 130.99 ± 4.60 Ma (Hauterivian). The recognition of dextral-oblique Early Cretaceous reactivation of faults related to the underlying and older Orcadian Basin highlights the importance of structural inheritance in controlling basin- to sub-basin-scale architectures and how this influences the kinematics of IMFB rifting.

Supplementary material: Analytical protocols and analysed sample details are available at https://doi.org/10.6084/m9.figshare.c.5635432

Received 28 May 2021; **revised** 12 September 2021; **accepted** 27 September 2021

Many sedimentary basins worldwide are superimposed partially or completely over the sites of older, pre-existing basins; for example, the Colorado Basin (Lovecchio *et al.* 2018), the East African Rift (Macgregor 2015; Ragon *et al.* 2018), the Gulf of Aden (Fournier *et al.* 2004), the NE Atlantic margin (Hansen *et al.* 2012; Henstra *et al.* 2019), the East Greenland rift system (Rotevatn *et al.* 2018), the North Sea Rift (e.g. Tomasso *et al.* 2008) and the West Orkney Basin (Wilson *et al.* 2010). The role of inherited structures is commonly difficult to constrain in such settings owing to the limited resolution of seismic data in offshore regions, whereas onshore areas may be limited by restricted surface exposure and lack of evidence to constrain the absolute age of fault movements, yet a better understanding of how earlier-formed faults localize deformation and interact during rifting can give key insights into basin development and potentially reduce subsurface uncertainties. One potentially useful approach is to focus on well-exposed coastal outcrops where structures imaged offshore can be traced directly or indirectly onshore. In many cases, individual faulting episodes will be associated with syntectonic mineral fills, such as calcite or base metal sulfides, which can then be dated using radiometric methods (e.g. U–Pb calcite) to constrain the age of specific faulting episodes (e.g. see approach used by Dichiarante *et al.* 2016; Roberts *et al.* 2020*b*). In particular, *in situ* laser ablation inductively coupled plasma mass spectrometry (LA-ICP-MS) U–Pb calcite dating has become highly popular in recent years. Calcite can incorporate uranium upon its formation, making it a potentially suitable chronometer for U–Pb and U–Th geochronology, allowing it to be used to provide direct timing constraints for a broad range of geoscience applications, including the timing of vein formation and crustal fluid flow (Kylander-Clark 2020; Roberts *et al.* 2020*a*). Using *in situ* LA-ICP-MS allows the targeting of specific microstructural features of carbonate-bearing fault rocks (Hoareau *et al.* 2020), giving a much more rigorous approach to calcite U–Pb dating of complex geological regions with multiple tectonic or fluid flow events.

This paper focuses on the nature, age and regional significance of faulting and fracturing present in the onshore Devonian succession of the southern Inner Moray Firth Basin (IMFB) and Orcadian Basin (Fig. 1a–c). New detailed field observations in the Turriff Sub-basin (Fig. 1c) coupled with U–Pb dating of synkinematic calcite mineralization are used to document and characterize the kinematic history of faulting. The latter is utilized to explore the role that inherited Devonian structures played in basin development during subsequent (Mesozoic and Cenozoic) deformation. These findings reveal hitherto unrecognized evidence for interactions

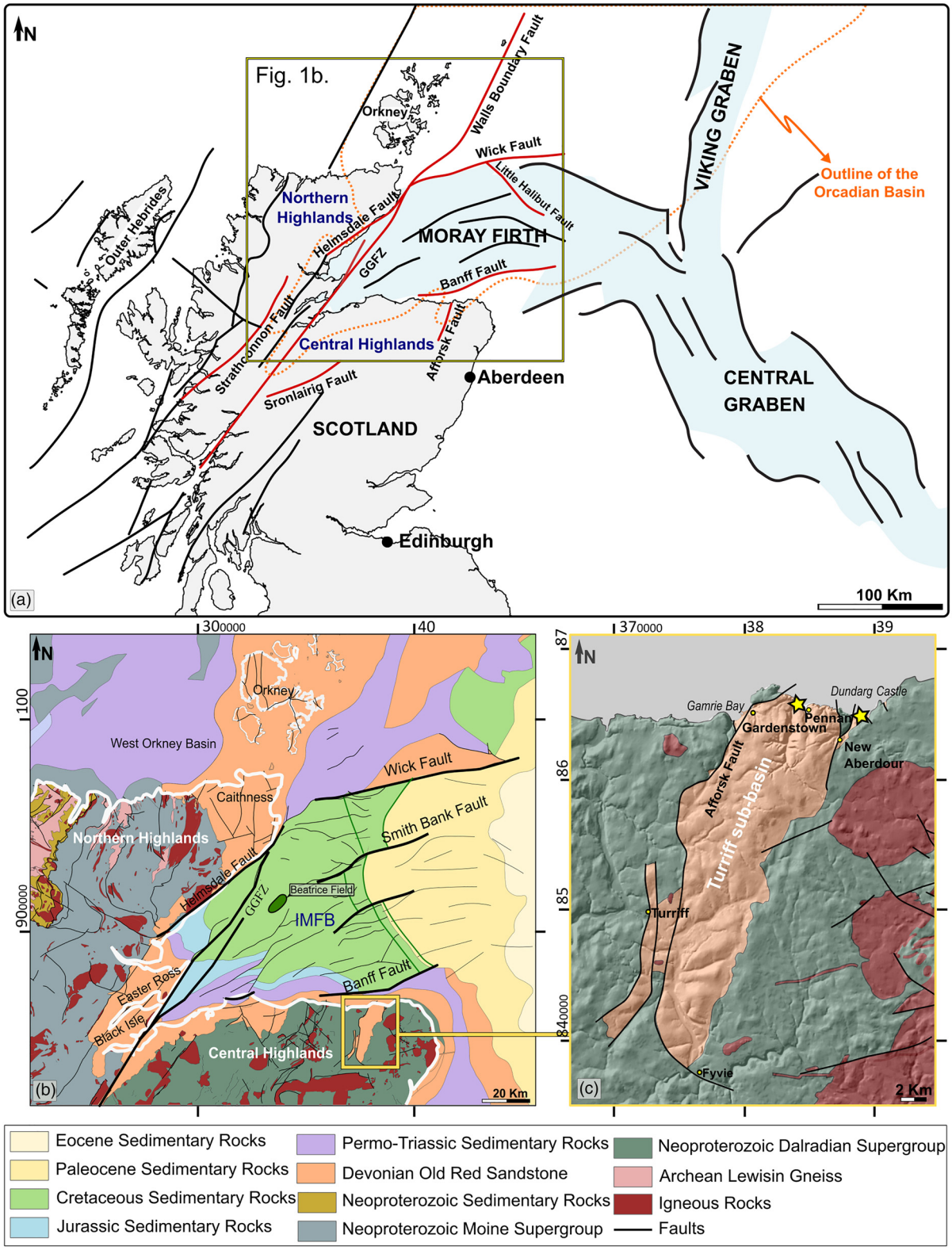

Fig. 1. (**a**) Simplified tectonic map of Scotland and the North Sea showing the main fault systems (after Roberts and Holdsworth 1999; Zanella and Coward 2003; Kemp *et al.* 2019). The faults mentioned in the text are shown in red. GGFZ, Great Glen Fault Zone. Outline of the Orcadian Basin is marked by a dotted orange line (after Duncan and Buxton 1995). (**b**) Regional geological map of northern Scotland and associated offshore regions showing the main stratigraphy and fault systems (modified after Guariguata-Rojas and Underhill 2017 and British Geological Survey (BGS), UK, using EDINA Geology DigimapService, http://edina.ac.uk/digimap). IMFB, Inner Moray Firth Basin. (**c**) Geological map of the Turriff sub-basin (modified after British Geological Survey (BGS), UK, using EDINA Geology DigimapService, http://edina.ac.uk/digimap). Yellow stars show location of the areas of study.

between younger rifting episodes and pre-existing sub-seismic-scale Devonian structures, providing a potential new structural template for interpretation of the subsurface basin architecture in the offshore IMFB and elsewhere.

Geological overview

The IMFB is a superimposed basin founded on Precambrian to Caledonian metamorphic basement and post-orogenic Devonian–

Carboniferous sedimentary rocks related to the Orcadian Basin. From Permian until Cretaceous times it forms the western arm of the intra-continental North Sea trilete rift system (McQuillin *et al.* 1982; Frostick *et al.* 1988; Andrews *et al.* 1990; Roberts *et al.* 1990; Underhill 1991; Thomson and Underhill 1993) that was created following a period of transient thermal doming in the mid-Jurassic (Underhill and Partington 1993). The basin is bounded by major faults, including the Banff Fault to the south, the Helmsdale and Great Glen faults to the NW, and the Wick Fault to the north (Fig. 1b). The IMFB changes eastwards into the Outer Moray Firth Basin, which links into the Central and Viking grabens in the central part of the North Sea. The IMFB is widely believed to record important episodes of Late Cretaceous- to Cenozoic-age regional uplift and faulting, including dextral reactivation of the Great Glen Fault and sinistral reactivation of the Helmsdale Fault (e.g. Underhill 1991; Thomson and Underhill 1993; Le Breton *et al.* 2013).

The Mesozoic IMFB overlies the Devonian successions occupying the southern part of the Orcadian Basin (Fig. 1b; Johnstone and Mykura 1989; Friend *et al.* 2000). The earlier basin is a predominantly fluvial and lacustrine, intracratonic feature belonging to a much larger system of Devonian–Carboniferous basins that extends northwards into Shetland, western Norway and eastern Greenland (Seranne 1992; Duncan and Buxton 1995; Woodcock and Strachan 2012).

The potential influence of older structures related to the Orcadian Basin on the geometry and kinematics of later IMFB opening has to date received little attention, partly owing to the poor resolution of offshore seismic reflection data at depth, or sparse well data. It has been speculatively suggested, based on offshore data, that Orcadian Basin structures may have been reactivated in the IMFB (e.g. Norton *et al.* 1987; Coward *et al.* 1989), but little compelling evidence for this inheritance has yet emerged and its potential importance remains uncertain.

Stratigraphic and structural setting

Orcadian Basin

The Lower Devonian, basal part of the Orcadian Basin fill is represented by synrift alluvial fan and fluvial–lacustrine deposits. These units are mostly restricted to the western onshore–offshore parts of the IMFB (Rogers *et al.* 1989) and some areas of Caithness (NIREX 1994), with excellent exposures of limited extent also seen in the Turriff Sub-basin on the southern coast at Pennan–New Aberdour (Figs 1b, c and 2; e.g. Coward *et al.* 1989). Here, the Lower Devonian rocks unconformably overlie or are faulted against Neoproterozoic basement of the Dalradian Supergroup. They are thought to have been deposited in a series of small fault-bounded grabens of limited extent (e.g. Friend *et al.* 2000). These strata are unconformably overlain by Middle Devonian synrift alluvial, fluvial, lacustrine and locally marine sequences. Rocks of this age dominate the onshore sequences exposed in Caithness, Orkney and Shetland (Marshall and Hewett 2003). They are, in turn, overlain by Upper Devonian post-rift fluvial and aeolian sedimentary rocks (Friend *et al.* 2000). Younger Carboniferous fills conformably overlie Devonian strata and are restricted to currently offshore regions of the Orcadian Basin. They comprise sandstones, conglomerates and sparse claystones and siltstones interpreted as

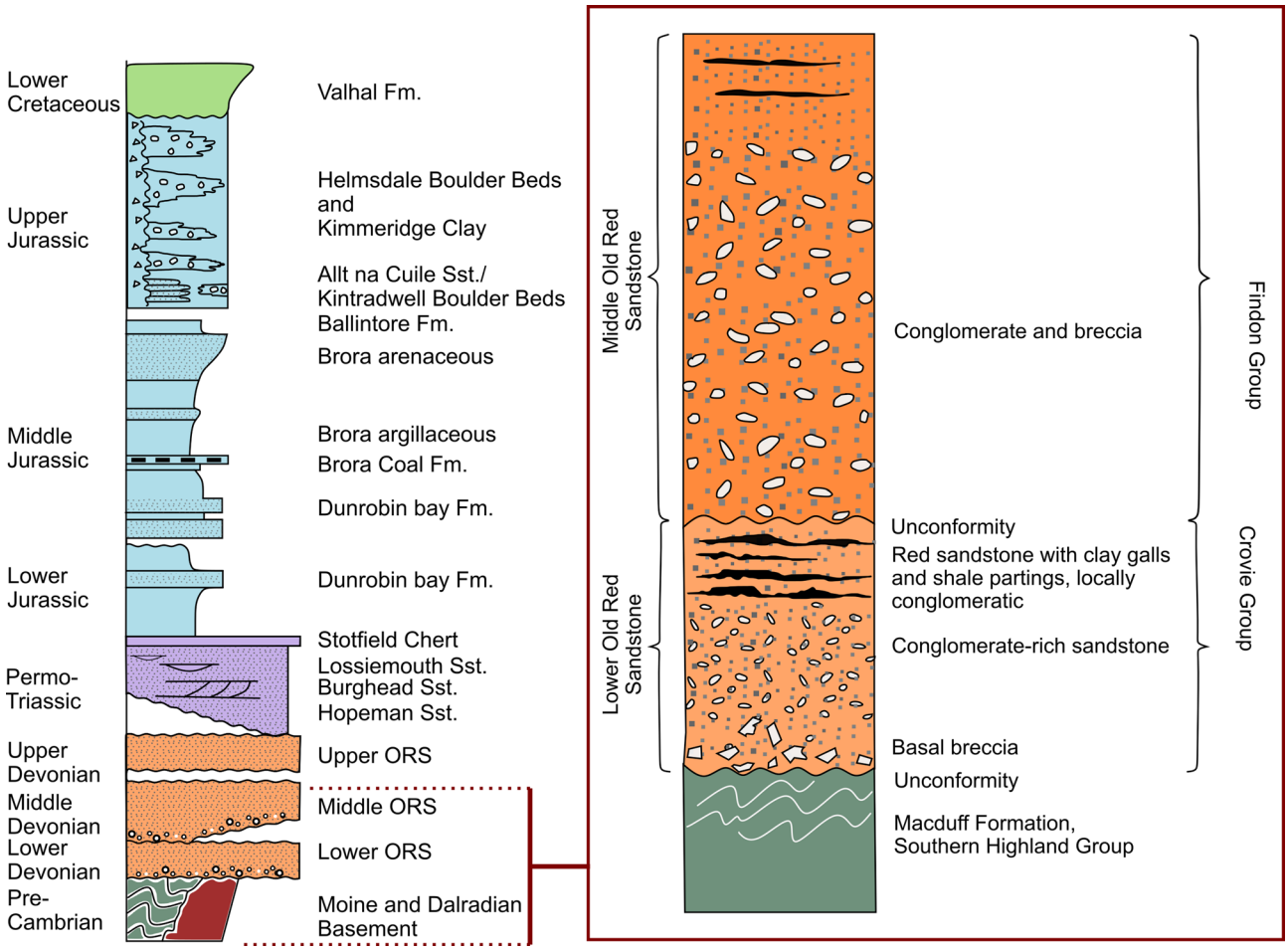

Fig. 2. Left-hand column shows the general stratigraphy of the IMFB (modified after Trewin and Hurst 2009) with details of the Devonian sequence redrawn after Gunn *et al.* (2015) shown in the inset right-hand column. Not to scale, with relative thicknesses shown being notional.

part of a regional fluvial depositional setting (e.g. Marshall and Hewett 2003).

The tectonic origin of the Orcadian and nearby West Orkney basins (Fig. 1b) has long been a matter of some controversy and debate. Interpretation of deep and shallow commercial seismic reflection profiles north of Scotland suggested that the West Orkney Basin comprises a series of half-grabens bounded by easterly dipping normal faults (e.g. Brewer and Smythe 1984; Coward and Enfield 1987). Earlier interpretations (e.g. McClay *et al.* 1986; Enfield and Coward 1987) postulated that much of the basin fill here was Devonian and that the Orcadian–West Orkney basins formed as a result of extensional collapse of the Caledonian orogen. More recent studies have cast doubt on these models, showing that the fill of the West Orkney Basin is mostly Permo-Triassic (e.g. Stoker *et al.* 1993) and that there is only limited onshore evidence for basement reactivation along the north coast of Scotland (e.g. Roberts and Holdsworth 1999; Wilson *et al.* 2010). Rifting in northern Scotland during the Devonian is now considered to be related to regional sinistral transtension during left-lateral shear along the Great Glen–Walls Boundary fault system (Seranne 1992; Dewey and Strachan 2003; Watts *et al.* 2007). However, Norton *et al.* (1987) argued against the dominance of strike-slip related development of the Orcadian basin and proposed a dip-slip evolution during NW–SE extension, and used the Turriff Sub-basin as one of their case studies to support their interpretation.

The Orcadian Basin later experienced a Late Carboniferous–Early Permian inversion event, thought to be related to dextral strike-slip movements along the Great Glen–Walls Boundary fault system (e.g. Coward *et al.* 1989; Seranne 1992; Watts *et al.* 2007; Wilson *et al.* 2010; Dichiarante *et al.* 2020). This led to regional-scale north–south folding and reverse reactivation of pre-existing Devonian graben-bounding faults from the Scottish mainland to Shetland (e.g. Underhill and Brodie 1993; Armitage *et al.* 2020; Dichiarante *et al.* 2020). In Caithness these structures are then everywhere crosscut by younger, predominantly normal faults formed during a later NW–SE rifting event (Wilson *et al.* 2010; Dichiarante *et al.* 2020). Dichiarante *et al.* (2016) used Re–Os geochronology to date base metal sulfides in syntectonic normal to transtensional fault infills and veins in Devonian rocks of the Dounreay area. These yielded a mid-Permian (267.5 ± 3.4 (3.5) Ma) age of faulting, which Dichiarante *et al.* (2016, 2020) argued was related to the development of the offshore West Orkney Basin located just the NW. Therefore, they viewed the latter basin as being younger, geographically separate and partially superimposed over the western flanks of the older Orcadian basin and its associated Devonian fills.

The Inner Moray Firth Basin

The stratigraphy of the IMFB (Fig. 2) is known from both surface (e.g. Hurst 1981; Pickering 1984; Frostick *et al.* 1988) and subsurface studies (e.g. Andrews *et al.* 1990; Roberts *et al.* 1990). The outcrops in onshore regions to the north and south are dominated by Precambrian basement rocks and Silurian–Devonian Caledonian intrusions that are unconformably overlain by Paleozoic (mainly Devonian, with lesser amounts of Permian strata) cover sequences (e.g. Johnstone and Mykura 1989; Stephenson and Gould 1995). Mesozoic strata (Triassic to Jurassic) have a limited extent onshore and occur almost entirely along coastal margins (Fig. 1b; e.g. Trewin 1987; Trewin and Hurst 2009). Offshore, the subcrop of the basin is dominated by Mesozoic–Cenozoic sedimentary rocks (Fig. 1b; e.g. Andrews *et al.* 1990; BGS 1995).

The IMFB is traditionally viewed as having opened during superimposed Permo-Triassic and Late Jurassic–Early Cretaceous rifting episodes, followed by episodes of subsidence, uplift and fault reactivation during the Late Cretaceous to Cenozoic (e.g. McQuillin *et al.* 1982; Underhill 1991; Thomson and Underhill 1993). The importance of Permo-Triassic rifting, which is widely recognized in other parts of the North Sea (e.g. Steel and Ryseth 1990; Bell *et al.* 2014; Fazlikhani *et al.* 2020), is debatable in the IMFB owing to poor resolution of seismic reflection data at depths where Permo-Triassic strata are imaged, sparse well data and limited onshore exposures. Early models suggested that during the Permo-Triassic, the basin evolved as a simple half-graben tilted against the Great Glen and Helmsdale faults (Frostick *et al.* 1988). Other researchers favoured a transtensional origin for the IMFB (e.g. McQuillin *et al.* 1982; Bird *et al.* 1987; Roberts *et al.* 1990). Such models typically assumed that the Great Glen Fault formed the main controlling structure and suggested that the basin opened as a result of dextral movements along this structure during NE–SW extension. McQuillin *et al.* (1982) estimated *c.* 8 km of displacement along the Great Glen Fault, which then generated 5–6 km of extension between the Wick and Banff boundary faults.

The transtensional models and the role of the Great Glen Fault during basin opening were challenged based on findings in a series of later studies (e.g. Underhill 1991; Thomson and Underhill 1993; Underhill and Brodie 1993). Largely on the basis of detailed interpretation of seismic profiles and construction of thickness maps between key stratigraphic intervals, Underhill (1991) proposed a new model for the evolution of the IMFB. He suggested that, after a long period of thermal subsidence during the Triassic to Middle Jurassic, the basin opened mainly during the Late Jurassic under an orthogonal extensional regime. The main displacements are interpreted to lie along the Helmsdale Fault, as the synkinematic sequence thickens without change across the Great Glen Fault and towards the Helmsdale Fault. This indicates that the former structure was inactive during the Late Jurassic. The widespread recognition of Jurassic-age syntectonic fault scarp breccias (locally termed the Boulder Beds) in the hanging wall of the Helmsdale Fault onshore, along the north coast of the IMFB, further supports fault activity at this time during basin opening (e.g. Trewin and Hurst 2009; McArthur *et al.* 2013). In contrast to the previously suggested oblique- or strike-slip deformation under a NE–SW stress regime (e.g. McQuillin *et al.* 1982; Andrews *et al.* 1990), Underhill (1991) proposed an orthogonal NW–SE to NNW–SSE extension direction across the Wick and Helmsdale faults. This is similar to the regime suggested by Davies *et al.* (2001) for the wider North Sea region during the Oxfordian and early Kimmeridgian, following a shift from east–west extension during the Bathonian and Callovian that generated north–south-trending structures in the Central Graben. The rifting in both the IMFB and wider North Sea is considered to be characterized by multiple stages of faulting separated by periods of near tectonic quiescence and is now generally thought to continue until the Early Cretaceous (e.g. Andrews *et al.* 1990; Davies *et al.* 2001; Zanella *et al.* 2003).

Limited information exists in the IMFB about a more detailed structural evolution and timing of fault activity, and it is also uncertain when rifting ended during the Early Cretaceous. Underhill (1991) suggested rifting up to the Berriasian followed by (post-Berriasian) onlap and regional subsidence in an under-filled basin. Davies *et al.* (2001) considered that during the Kimmeridgian and Volgian, mainly NW–SE-trending faults developed under a NE–SW rifting direction, and that this extension ceased in the Berriasian. Andrews *et al.* (1990) implied that rifting continued until later in the Early Cretaceous based on the preservation of thick (1.6 km) Valanginian to Albian synrift deposits in the hanging wall of the Little Halibut Fault (Fig. 1a). Roberts *et al.* (1990) identified the first reflector onlapping the synrift strata in the western part of the IMFB as near top Hauterivian. Argent *et al.* (2002) suggestedd that the Smith Bank fault was active until the Hauterivian. It is generally agreed, however, that following the cessation of rifting, the basin then

experienced a period of thermal subsidence during the Late Cretaceous (e.g. Andrews *et al.* 1990; Underhill 1991).

From the early Cenozoic to the present day, the IMFB is thought to have experienced episodes of uplift with regional erosion and eastward tilting, with some major faults undergoing reactivation (e.g. Underhill 1991; Argent *et al.* 2002). These events have been variously related to the uplift caused by the regional development of the early Iceland mantle plume, the far-field effects of the Alpine Orogeny, or plate readjustment during the opening of the North Atlantic rift (see Le Breton *et al.* 2013, and references therein). The Great Glen Fault is believed to be the major controlling structure in the basin at this time (Underhill 1991). Offshore, seismic reflection profiles show evidence for the development of strike-slip-related deformation patterns including flower structures, folds and offset post-rift reflectors (e.g. Thomson and Underhill 1993; Underhill and Brodie 1993; Davies *et al.* 2001). Onshore evidence of Cenozoic structures supposedly includes the development of large-scale folds, of about 500 m wavelength trending NW–SE, in the hanging wall of the Helmsdale fault (Thomson and Underhill 1993; Thomson and Hillis 1995). In addition, minor folds and faults in the Jurassic strata exposed at Black Isle and Easter Ross (Fig. 1b) are considered to be Cenozoic and related to right-lateral slip of the Great Glen Fault (e.g. Underhill and Brodie 1993; Le Breton *et al.* 2013). The effects of Cenozoic deformation away from Great Glen Fault are less certain.

Turriff Sub-basin

Our study area lies in part of the north–south-trending Turriff Sub-basin (Fig. 1c), one of the largest Devonian outliers in the onshore Central Highlands (e.g. Stephenson and Gould 1995). The basin extends for *c.* 11 km along the southern coast of the IMFB from Gamrie Bay at Gardenstown to Dundarg Castle at New Aberdour Bay and extends inland and southwards *c.* 40 km to Fyvie (Fig. 1c). This location was chosen for study because of the relatively good coastal exposures, and because it presents a better opportunity to characterize both the Devonian and Mesozoic deformation patterns that are widely overprinted and obscured on the northern margins of the IMFB owing to the effects of later supposedly Cenozoic reactivation along the Great Glen Fault zone (e.g. Le Breton *et al.* 2013).

The Turriff Sub-basin is a Devonian half-graben, bounded to the west by the Afforsk Fault whereas the eastern side is both faulted and locally unconformable on the Dalradian metamorphic basement (Fig. 1c; e.g. Read 1923; Ashcroft and Wilson 1976; Trewin 1987). The stratigraphy, sedimentology and interpretation of depositional environments have been studied in some detail and it is generally agreed that the basin fill consists of both Lower and Middle Devonian rocks, assigned, respectively, to the Crovie and Findon groups (Fig. 2; e.g. Read 1923; Trewin 1987). An angular unconformity, considered the boundary between the two groups, is exceptionally well exposed at Pennan (Fig. 1c; BGS 1987; Trewin 1987; Gunn *et al.* 2015). The succession, having a total thickness of up to 800 m in the northern part and 1400 m in the southern part of the basin (e.g. Gunn *et al.* 2015), is dominated by breccias and conglomerates, with minor sandstones and mudstones, all of which show marked lateral facies variations. Both successions are interpreted to belong to alluvial fan systems with adjacent mudflats and playa lake deposits (e.g. Sweet 1985; Trewin 1987; Trewin *et al.* 1987). The breccias and conglomerates of the Crovie Group contain granitic and felsitic clasts, whereas the Findon Group is dominated by clasts derived from the local Dalradian Macduff Slate (Trewin 1987).

The structural style of the Turriff Sub-basin is regarded as complex, especially on the IMFB coast (Ashcroft and Wilson 1976). The bedding is mostly gently westward dipping (e.g. Sweet 1985; Trewin 1987; Gunn *et al.* 2015), but Read (1923) in his detailed work noted a greater variability of dips. Several fault networks have been recognized based on surface geological mapping (e.g. Read 1923; Sweet 1985; Trewin 1987), gravity data (Ashcroft and Wilson 1976) or interpretation of nearby offshore seismic reflection profiles (e.g. Norton *et al.* 1987). The dominant fault strikes are predominantly NNE–SSW, parallel to the basin margins (e.g. Ashcroft and Wilson 1976; Sweet 1985; Trewin 1987; Coward *et al.* 1989). Ashcroft and Wilson (1976) interpreted fault development to have occurred during Devonian rifting based on comparisons with other parts of NE Scotland. Norton *et al.* (1987) suggested that the Devonian faults were highly arcuate along ESE–WNW, ENE–WSW and north–south trends. They proposed an overall NW–SE extension direction during the Devonian that would require a significant strike-slip component to occur along the segments of these faults that are obliquely oriented to the inferred rifting vector.

A younger set of faults trending ENE–WSW (e.g. Sweet 1985; Trewin 1987) were considered by Ashcroft and Wilson (1976) to have initiated during Permo-Carboniferous times, based on the observation that a dyke swarm interpreted by Buchan (1932) to be of that age has a similar trend across NE Scotland. These researchers also noted that this ENE–WSW trend is approximately parallel to the southern margin of the IMFB and suggested that movements along structures with this trend continued into the Mesozoic.

Methods

Fieldwork and stress inversion analyses

The field data described in this study focus on the Lower and Middle Devonian coastal outcrops of the onshore Turriff Sub-basin (Fig. 1c). Kilometre-long exposures of Crovie and Findon groups (Read 1923; Trewin 1987) in the central and eastern part of the sub-basin show representative sequences of events and variety of brittle deformation structures. The outcrops are referred to as the Pennan and New Aberdour localities (Fig. 1c) here, based on their proximity to nearby villages.

In situ detailed field observations and measurements of bedding, faults, fractures, folds, fault rocks and associated mineralization were recorded. Where accessible, the structural measurements were taken using both a Suunto geological compass–clinometer and the FieldMove™ digital mapping application on an Apple iPad™ (sixth generation). At each locality studied, the relative ages of structures were carefully assessed using cross-cutting relationships. The sense of fault movement was determined based on the presence of offset stratigraphic markers and kinematic indicators such as slickenlines, in addition to shear sense criteria such as asymmetric, en echelon arrays of Riedel or tensile veins (e.g. Petit 1987).

Structural data processing and visualization were carried out using Stereonet 10 (Allmendinger *et al.* 2012; Cardozo and Allmendinger 2013). The measurements were graphically represented using both rose diagram plots of azimuth distributions (at 10° sector angles) and equal area stereonets, lower hemisphere projection using poles to planes where appropriate. The contouring was calculated after Kamb (Kamb 1959) at 2 and 3 sigma standard deviation above a random population.

Fault-slip slickenline data were collected *in situ* from exposed fault surfaces to perform a palaeostress inversion. This analysis assumes that slip on a fault surface occurs in the direction of the maximum resolved shear stress (Wallace 1951; Bott 1959). Numerous methods have been developed to invert fault kinematic data and derive palaeostress (e.g. Spang 1972; Angelier 1984, 1990; Michael 1984; Mostafa 2005) by obtaining the orientation of the three principal stress axes (σ_1, σ_2 and σ_3, which are the maximum, intermediate and minimum principal stress, respectively) and the stress ratio (R), which is defined as $(\sigma_1 - \sigma_2)/(\sigma_2 - \sigma_3)$, also called

the reduced stress tensor. In this study, the fault data were analysed using the direct inversion method (INVD) of Angelier (1990) implemented using the SG2PS software (Sasvári and Baharev 2014). This method estimates the reduced stress tensor and the shear stress magnitudes from the fault-slip data (Angelier 1990). The program also graphically computes the stress regime based on the stress index (R') (Delvaux *et al.* 1997). The stress index is based on the identity of the vertical stress axes and the stress ratio as follows: radial extension (σ_1 vertical, $0 < R < 0.25$); pure extension (σ_1 vertical, $0.25 < R < 0.75$); transtension (σ_2 vertical, $0.75 < R < 1$ or σ_2 vertical, $1 > R > 0.75$); pure strike-slip (σ_2 vertical, $0.75 > R > 0.25$); transpression (σ_2 vertical, $0.25 > R > 0$ or σ_3 vertical, $0 < R < 0.25$); pure compression (σ_3, vertical, $0.25 < R < 0.75$); and radial compression (σ_3 vertical, $0.75 < R < 1$). The stress index is expressed numerically as continuous values between zero and three, where values ranging from zero to one are defined for extensional stress regimes (R' = R, σ_1 is vertical), one to two for strike-slip stress regimes (R' = 2 – R, σ_2 is vertical) and from two to three for compressional stress regimes (R' = 2 + R, σ_3 is vertical) (for more details see Delvaux *et al.* 1997).

Photogrammetry

Photogrammetry, especially unmanned aerial vehicle (UAV-)based photogrammetry, is a valuable and increasingly used technique as it allows a visual assessment of the spatial distribution of structures across a wide range of scales (centimetres to kilometres) and gives greater access to otherwise inaccessible parts of the outcrop in cliffs. It also allows the routine extraction of structural observations and data from 3D digital outcrop models (DOM) (e.g. McCaffrey *et al.* 2005; Weismüller *et al.* 2019; Tămas *et al.* 2021). In our case, the acquisition of UAV photography was made using a DJI Mavic Air drone, which has a digital camera with a 12-megapixel image sensor.

For horizontal exposures, we used a pre-set automated flight path and data acquisition process. This was achieved with the use of Pix4Dcapture software, used with an Apple iPad (sixth generation). The acquisition parameters were a front overlap of 80%, a side overlap of 70% and a 70° camera angle. The altitude of acquisition varied between a few centimetres and 50 m. For the vertical or steeply inclined cliff exposures, we used a manual flight path and image acquisition process. The camera was oriented orthogonal to the exposure and we tried to achieve a similar level of overlap to the automated acquisition.

For the creation of the DOM, digital elevation models (DEM) and orthorectified models, we used Agisoft Metashape Professional™ (v.1.6.2). The process of constructing the models involves a series of steps to create an accurate photograph alignment, which then leads to the development of a sparse point cloud, followed by the creation of a dense point cloud, mesh and texture. The 3D textured meshes (DOM), together with the dense point cloud data, were imported into Virtual Reality Geological Studio (VRGS v.2.52) software (Hodgetts *et al.* 2007) to allow structural interpretation and extraction of structural orientation data. These included bedding, fault and fracture orientations. Where presented together with structural data collected by hand, these readings are shown in a different colour on stereoplots. To reduce uncertainties regarding the positioning and orientation of the 3D outcrops and orthomosaics, several orientation measurements were ground-truthed. The orthomosaic orientation has also been cross-checked with satellite imagery data. Lineament orientation analysis was performed using FracPaQ (Healy *et al.* 2017), a MATLAB-based toolbox.

Microscopy and U–Pb geochronology

Structurally oriented samples of calcite mineral fills associated with specific fault zones recognized during fieldwork were collected for microscopic and geochronological analysis. U–Pb analysis of four calcite fracture fills was undertaken at the University of Hull using *in situ* LA-ICP-MS. Ablation was carried out using an Applied Spectra, RESOlution-SE 193 nm laser with a Laurin Technic S155 two volume cell, laser wavelength of 193 nm, pulse width of 5 ns, fluence of 5 J cm^{-2}, repetition rate of 10 Hz, ablation time of 30 s and 100 µm spot size. Helium and N_2 were used in the cell with Ar acting as the main carrier gas. Isotopic analyses were carried out using an Agilent 8800 ICP-MS system with an RF power of 1170 W and nebulizer gas flow of 0.86 l min^{-1} with the electron multiplier in counts per second mode. All samples were tested and mapped for uranium content to ascertain whether they contain sufficient abundance of ^{238}U to yield a Model 1 U–Pb discordia age. Isotopic mapping was carried out on polished chips with a fluence of 5 J cm^{-2}, on laser energy of 6.4 mJ, square 80 × 80 µm spot size and a scan speed of 20 µm s^{-1} with a repetition rate of 10 Hz. All uncertainties were propagated in the Iolite software package following the approach used by Holdsworth *et al.* (2020) . The Iolite software uses the reference standard analyses to estimate the propagated analytical uncertainty. This is done by individually removing each analysis and treating it as an unknown, which results in a population of pseudo-secondary standards. It does not address any potential sources of bias (e.g. nonmatrix matched standards, or measurement biases between zircon standards). Uncertainties are further propagated through the addition of the standard reference material uncertainties in quadrature. The U–Pb data are presented on Tera–Wasserburg plot and a Model 1 age is calculated (with age and $Pb_{initial}$ uncertainties quoted as 2σ) using IsoplotR (Vermeesch 2018).

Only one sample (S02) contained sufficient ^{238}U abundance (and low common lead values) to yield an accurate and precise date. A further sample (S01) was also analysed at the BGS Isotope Geosciences Laboratory, but did not contain sufficient amounts of ^{238}U compared with common lead to yield suitable U/Pb ratios to produce a geologically meaningful date. Analytical protocols and analysed sample details are provided in the Supplementary Materials.

Thin sections were studied and photographed using an optical transmitted light microscope to ascertain the relative age of the mineral fills, any fault-related displacements and deformation. A key requirement here was to demonstrate that the growth of calcite could be shown to be synchronous with fault displacements recognized during fieldwork. Thin sections from three representative samples from New Aberdour (S01–S03) are used in this paper to illustrate our findings.

Results

Fieldwork

Pennan [NJ 845 654]

The village of Pennan lies in a central location along the coastal outcrop of the Turriff Sub-basin Devonian fill (Fig. 1c). The exposure studied here is about 1 km long and extends from Millshore [NJ 84059 65813] to Pennan Harbour [NJ 84716 65551] (Fig. 3a). The exposure comprises limited wavecut platforms and very good coastal cliff exposures 10–25 m high, which are fully accessible at intermediate and low tides. The rocks exposed belong to both the Crovie and Findon groups (Fig. 2; Read 1923; Trewin 1987). Both sequences here are predominantly composed of red conglomerates, breccias and sandstones, and are interpreted to have formed in alluvial fan systems (e.g. Trewin 1987). The Findon Group is generally coarser grained, and is dominated by metre-thick breccias with angular and subangular centimetre- to decimetre-scale fragments of Dalradian basement (Macduff Slates). Only a few centimetre-thick layers of medium–coarse red-coloured sandstone,

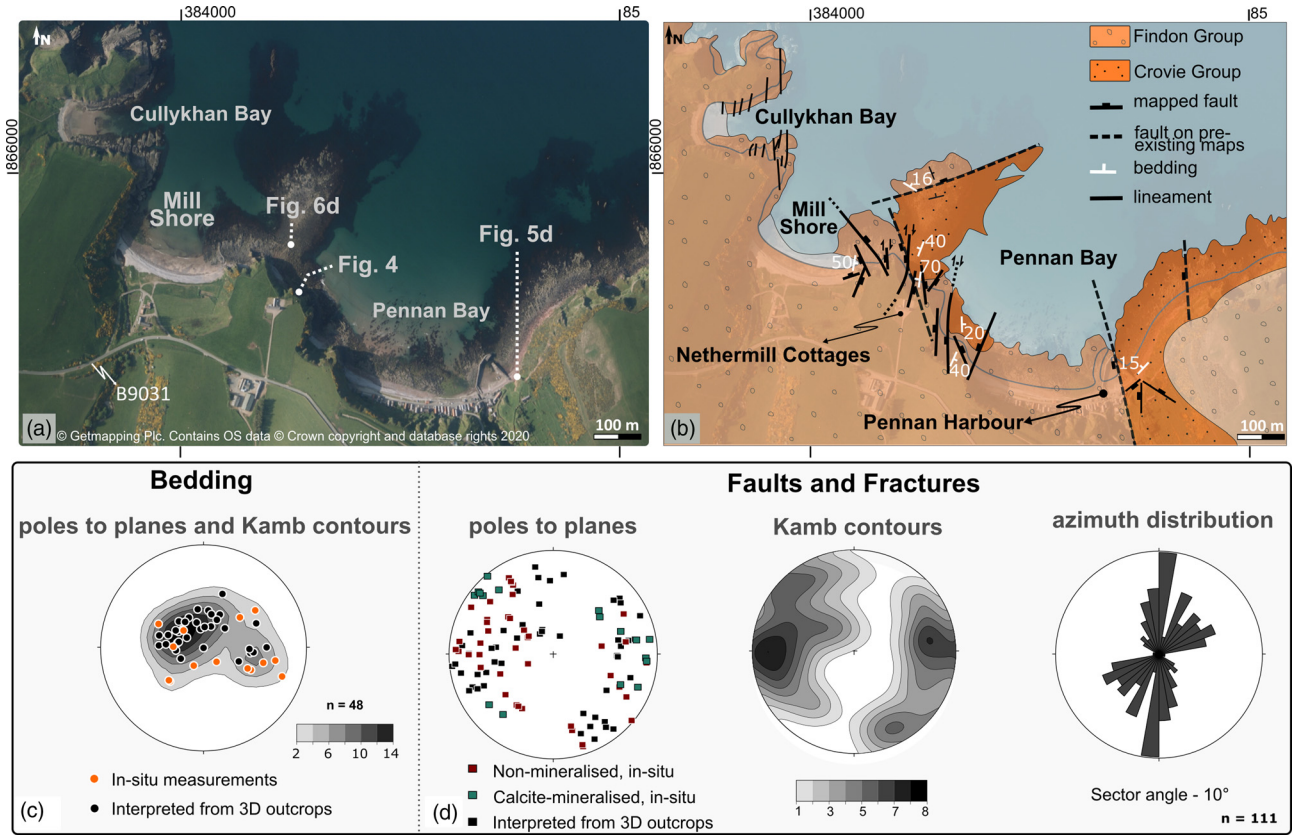

Fig. 3. (**a**) Aerial map (using EdinaDigimap service © Getmapping Plc) and (**b**) geological map of Pennan. Field data supplemented with data digitized after Trewin (1987). (**c**) and (**d**) Stereonets and rose plots of structural data collected in the field. Lower hemisphere, equal area projections. The locations of Figures 4–6 are also shown in (**a**).

usually lensoid (e.g. Fig. 4b and c), can be observed, whereas in the older Crovie Group red-coloured sandstones are better developed. The sandstone beds here can be more than 1 m thick, but are more usually 10–50 cm in thickness (e.g. Figs 4b and 5). In the cliff exposure close to Pennan harbour (Figs 3b and 5c), they form a sandstone-dominated sequence with a vertical extent of at least 25 m. East of Millshore, below the Nethermill Cottages [NJ 84255 65724], an angular unconformity between the Crovie and Findon groups is beautifully exposed in coastal cliff and foreshore exposures (Fig. 4; see also Norton *et al.* 1987; Trewin 1987). This location is traditionally considered to be the only place within the Orcadian Basin where an angular unconformity between the Lower and Middle Devonian sequences can be directly observed (e.g. Norton *et al.* 1987).

In both the Crovie and Findon groups, bedding orientations are variable, dipping gently to steeply (*c.* 15° to 70°) usually towards the east or west, and more locally in other directions (Fig. 3c). Close to Millshore, the bedding dips mainly *c.* 30° to 50° east or ESE (Fig. 3b). Walking east, in the cliffs below Nethermill Cottages the dips steepen to 70° and are usually inclined towards the west, whereas about 100–150 m from the cliffs to the north in the wavecut platform, the dips are shallower and are generally towards the NE (Fig. 3b). The beds are also more gently dipping NW on the eastern side of Pennan Bay, close to the harbour (Fig. 3b).

The Crovie and Findon groups are crosscut by numerous, commonly closely spaced (decimetre to metre separation) faults, fractures or fracture corridors and veins (e.g. Figs 4–6). Fault displacement histories are complex, but most faults show a significant component of normal movement based on offsets of bedding markers. The main sets of faults and fractures have two preferred orientations. The dominant set trend broadly north–south (*c.* 30° scatter) dipping both east and west, whereas a second set trend NE–SW (*c.* 60° scatter) (Fig. 3d). The normal fault planes typically have high to subvertical dips (60–88°), but less common, shallowly dipping faults of about 20–40° are also encountered locally (Fig. 3d).

In the cliffs below the Nethermill Cottages, the angular unconformity between the Lower and Middle Devonian is spectacularly exposed in an outcrop 15 m wide and 20 m high, forming a local half-graben tilted towards the east (Fig. 4a). The sequence is affected by a series of decimetre- to metre-spaced normal offset faults (e.g. Fig. 4b and c). The amount of offset along individual faults is usually difficult to quantify owing to the lack of stratigraphic markers, but where it can be observed, faults show dip-slip displacements ranging from a few centimetres (e.g. Fig. 5a) to several metres. Clear thickening of the strata can be observed in the hanging walls of faulted units both below and above the unconformity, illustrating the persistent and synkinematic nature of growth faulting during deposition of both the Crovie and Findon group strata (Figs 4 and 5a). Whereas some growth faults do not pass up into the younger Middle Devonian succession, others clearly do continue and also show growth thickening of beds into fault hanging walls within the younger stratigraphy (Fig. 4). The faulted blocks show locally significant amounts of rotation (*c.* 40°), and this has contributed to the markedly angular nature of the unconformity developed between what are considered to be Lower and Middle Devonian strata (e.g. BGS 1987; Trewin 1987). The prominent low-angle fault (highlighted in bright red) at the base of the outcrop in Figure 4 shows growth strata both in the hanging wall (Fig. 4b and c) and (apparently) in the footwall (Fig. 5a). This aspect can be explained by subsequent cross-cutting faulting and block rotation (Fig. 5c).

Close to Pennan harbour, a previously mapped (e.g. Trewin 1987; BGS 1995) major north–south-trending fault juxtaposes Middle

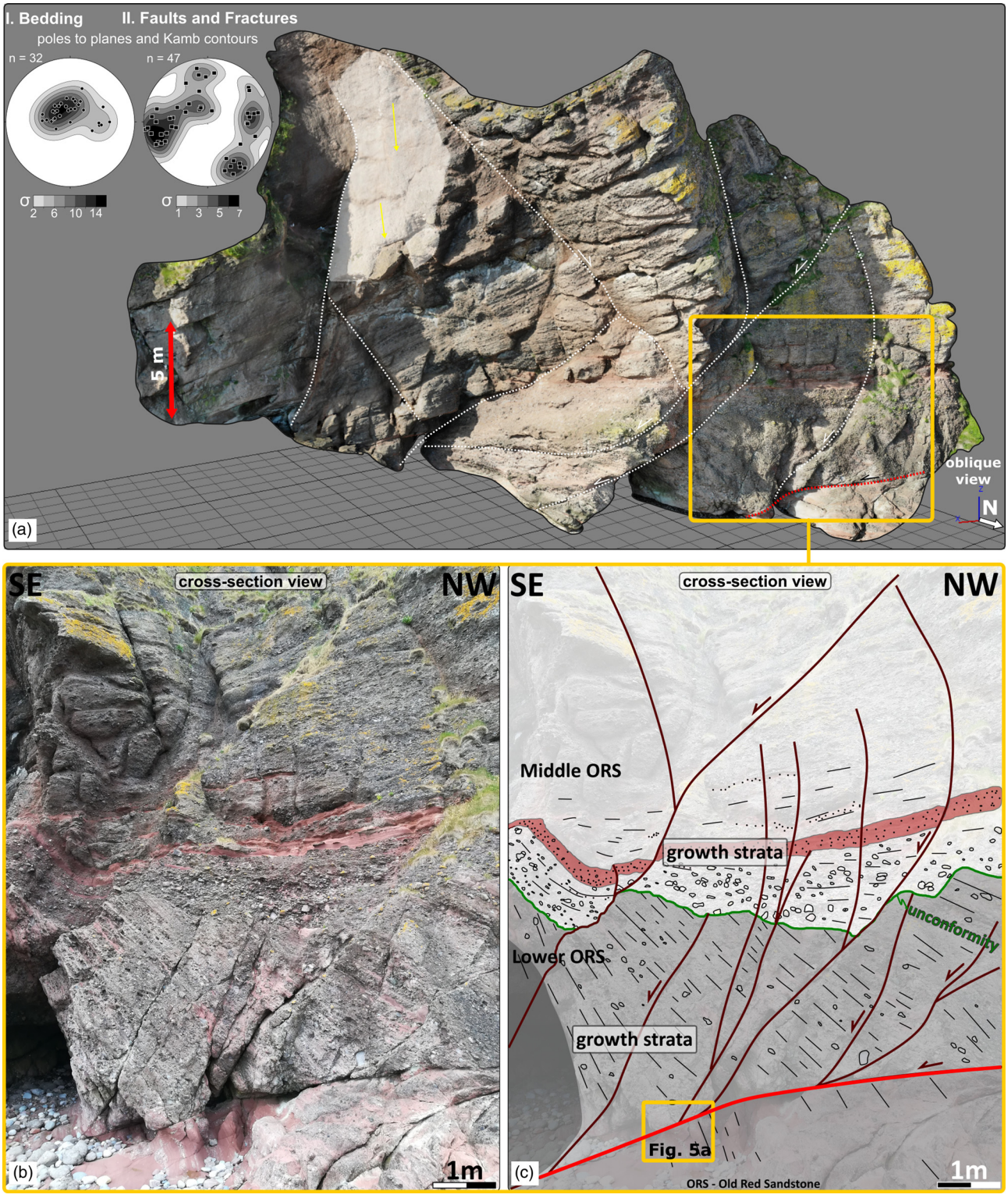

Fig. 4. Cliff exposure below the Nethermill Cottages; location is indicated in Figure 3a. (**a**) Three-dimensional digital outcrop and inset lower hemisphere equal area stereonets derived from planes extracted from 3D photogrammetric model. Main faults are highlighted in white with senses of offset where known. Lineations on fault plane are shown by yellow lines. Locations of (**b**) and (**c**) are indicated by the yellow box. (**b**) Field photograph and (**c**) line drawing showing a cross-sectional view looking SW onto the angular unconformity between the Lower and Middle Devonian and main faults with growth strata in their hanging wall. The low-angle fault at the base of the outcrop should be noted. The location of Figure 5a is shown by the yellow box.

Devonian hanging-wall strata to the west against a Lower Devonian footwall to the east (Fig. 3b). The fault core is not exposed, but about 70 m east in the footwall of the fault, a *c.* 10 m wide fault-parallel deformation zone is exposed. It is characterized by multiple decimetre-spaced faults and fractures (Fig. 5d). Most are shallow to steeply dipping (*c.* 10–85°), NW–SE-trending structures. Here, the low-angle planes appear to be more shallowly dipping segments of a series of curved or listric geometry faults, which have higher dips in the upper part, decreasing to (near) horizontal downdip (e.g. Fig. 5d).

The fault rocks and mineral fills associated with the brittle structures identified at Pennan can be divided in two main types. The first group comprises fault zones characterized by sharply defined, clean breaks (e.g. Fig. 5a, d and e), sometimes associated

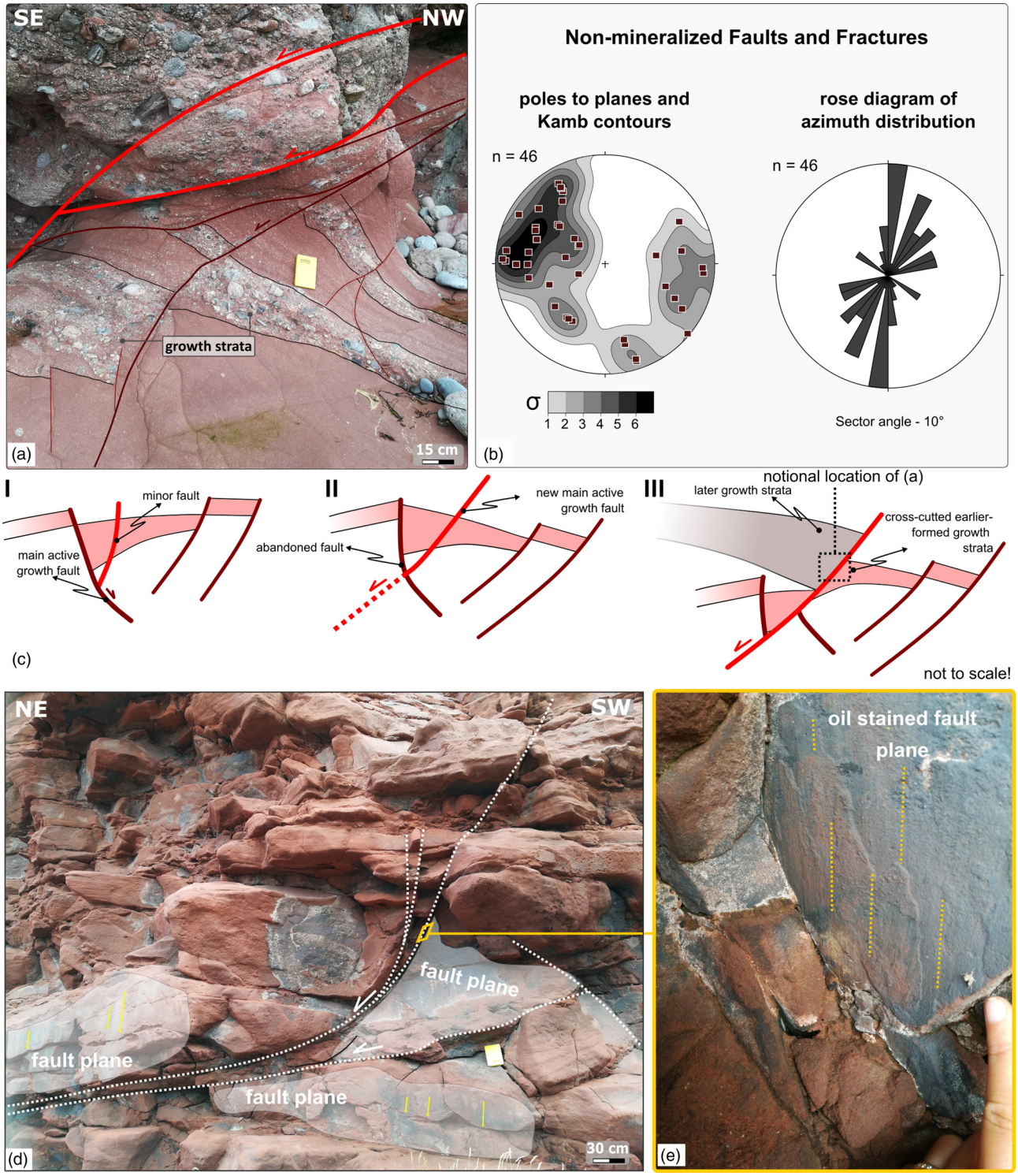

Fig. 5. Non-mineralized faults and fractures at Pennan locality. (**a**) Oblique view showing growth packages within the tilted Lower Devonian sequence. The non-mineralized faults are highlighted in red (see location in Fig. 4b). (**b**) Stereonet and rose plot of the non-mineralized faults and fractures at Pennan. (**c**) Sketch explaining the presence of growth strata in the footwall of the bright red coloured fault in Figure 4 and in (**a**). (**d**) Field photograph showing low-angle and listric faults in the Lower Devonian exposure at Pennan Harbour (see location in Fig. 3a). (**e**) Oblique view of an exposed non-mineralized fault plane showing dip-slip kinematics. In places, oil stains are visible on the fault or fracture planes.

with decimetre-thick fault breccia infilling dilatant jogs, and dark red or green gouges. We refer to these as 'non-mineralized faults'. The other fault group is marked by the development of calcite-cemented breccias (Fig. 6a and b), calcite tensile veins (Fig. 6d) and calcite slickenfibres developed along shear plane surfaces. We refer to these as 'calcite-mineralized faults'.

The non-mineralized faults predominantly trend north–south to NNE–SSW and NW–SE (Fig. 5b). Although kinematic indicators are uncommon, slickenline lineations and grooves are sometimes preserved, especially in finer-grained units of the Crovie Group (e.g. Fig. 5d and e). The fault panels of north–south- to NNE–SSW-trending structures typically show dip-slip to sinistral-oblique kinematics (*c.* 50–85° pitch), whereas the NW–SE-trending faults are usually dip-slip (80–90° pitch; e.g. Fig. 5d, e).

The calcite-mineralized faults and veins predominantly trend NE–SW, but north–south- to NNE–SSW- or NW–SE-trending

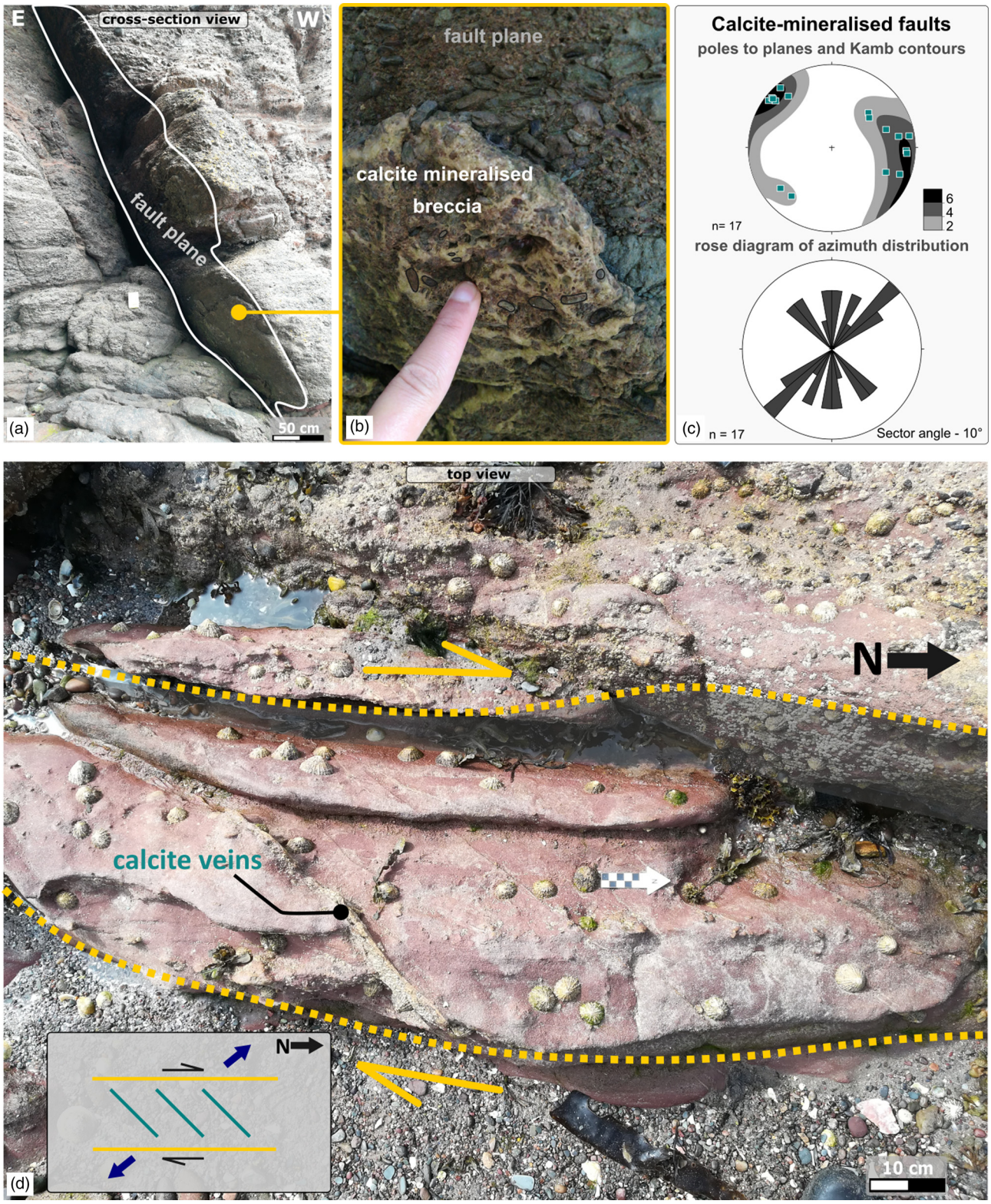

Fig. 6. Calcite-mineralized faults, fractures and associated structures at the Pennan locality. (**a**) Cross-section view of a north–south-trending calcite-mineralized fault. (**b**) Detailed image of calcite-mineralized breccia in the fault core. (**c**) Stereonet and rose plot of calcite-mineralized faults and fractures (lower hemisphere, equal area projection). (**d**) Oblique view and sketch of tensile calcite veins associated with a north–south-trending fault indicating dextral slip along the fault.

faults are also present (Fig. 6c). Calcite mineralization is mainly seen in patches, cementing the breccia in fault zones (Fig. 6a and b) or in adjacent wall rocks forming tensile veins of less than 1 mm to several centimetres thick (Fig. 6d). The NE–SW trend is well represented by tensile veins observed in close proximity to north–south-trending faults (Fig. 6d). A key feature of the calcite-mineralized faults is that, in contrast to the non-mineralized structures, the north–south- to NNE–SSW-trending faults show dextral to oblique-dextral or normal kinematics. This is indicated both by slickenlines identified on the fault panels and also by asymmetrically associated tensile veins arranged in en echelon arrays. Figure 6d shows an example of oblique dextral slip

associated with one of the major north–south-trending, steeply dipping faults (80/270) which can be traced in both the cliffs and wave-cut platform. The fault is associated with en echelon, calcite-mineralized tensile veins trending NE–SW (Fig. 6d.) suggesting a component of dextral slip during NNE–SSW extension (Fig. 6d inset).

New Aberdour [NJ 884 633]

The village of New Aberdour lies on the coast about 7 km east of Pennan. The area is located close to the eastern margin of the Turriff Sub-basin (Fig. 1c). The investigated exposures extend about 1.5 km along the shoreline of New Aberdour Bay [NJ 885 646]. A flat-lying wave-cut platform 150–200 m wide, which is accessible at low tide, is present on the west side of the bay (e.g. Figs 7a and 8), whereas towards the east, both flat-lying platforms and cliffs up to 25 m high are exposed.

The exposed Lower Devonian rocks belong to the Crovie Group (e.g. Sweet 1985; Fig. 7b). On the easternmost side of the bay, the succession unconformably overlies Dalradian basement rocks (Fig. 2b) and comprises metre-thick beds of light red, poorly sorted breccias with angular to sub-angular clasts of Dalradian basement rocks (mainly andalusite and biotite schist), interpreted to have formed as debris-flow deposits laid down in alluvial fan systems (lithology 6, Fig. 7b; e.g. Sweet 1985; Trewin *et al.* 1987). The succession continues to the west as medium-grained fluviatile sandstones that are conglomeratic at the base and preserve trough cross-bedding locally (lithology 5, Fig. 7b). Based on palaeocurrent data, Sweet (1985) suggested that the sediments gradually filled a NNE–SSW-trending palaeo-valley. This sequence is overlain by a metre-thick bedded conglomeratic sequence (lithology 4, Fig. 7b) that becomes thinner-bedded and dominated by sandstones (lithology 3) representing proximal and distal alluvial fan environments, respectively (Sweet 1985). This, in turn, passes upwards into a sequence of centimetre-thick, fine-grained sandstones, laminated red and green mudstones, and limestones (lithology 1 and 2, Fig. 7b). They have been interpreted as alluvial plain or playa lake deposits (e.g. Sweet 1985; Trewin *et al.* 1987).

Overall, the beds are typically subhorizontal to gently dipping (02–30°) to the WNW but, as seen at Pennan, steeper dips (up to 55°) and a variety of dip directions are encountered locally (Fig. 7b and c). The sequence is crosscut by numerous faults, fractures and veins of variable orientations (Fig. 7b–d). These display components of normal offset along faults where this can be determined from offsets of stratal marker horizons.

A large (50 000 m^2) high-resolution orthorectified model (Fig. 8a) and DEM (Fig. 8b) obtained from UAV photography were acquired from the western side of the bay and allowed a lineament analysis to be performed that revealed the dominant structural trends. The interpretation was verified with field observations to ensure that the picked lineaments corresponded to faults, fractures and veins. A total of 102 lineaments of more than *c.* 10 m length were interpreted within the entire area of the model (Fig. 8c), and 328 lineaments of less than 10 m were measured on a smaller, well-exposed area of about 225 m^2 (Fig. 8d). At larger scales, NNW–SSE to NNE–SSW trends dominate, with subordinate NE–SW- and east–west- to SE–NW-trending structures also present (Fig. 8c.). At smaller scales, the ENE–WSW trend (40° scatter) is better represented, but lineaments trending NNW–SSE to NNE–SSW also occur (Fig. 8d).

Similar to the Pennan locality, the faults and fractures imaged and directly measured in the field can be subdivided into non-mineralized and calcite-mineralized groups. The non-mineralized faults trend ESE–WNW and north–south to NE–SW (Fig. 9a–c). The fault zones are characterized by sharply defined clean breaks (e.g. Fig. 9b), red or green millimetre to centimetre thick gouges (Fig. 9a) or centimetre to decimetre thick fault breccias. Kinematic indicators such as slickenline lineations and grooves are sometimes preserved on exposed fault panels (e.g. Figs 9b and 10c). On ESE–WNW-trending faults, the kinematic indicators are rarely visible. Only one fault preserved indications of normal, dextral oblique-slip kinematics. On north–south to NNE–SSW trends slickenlines

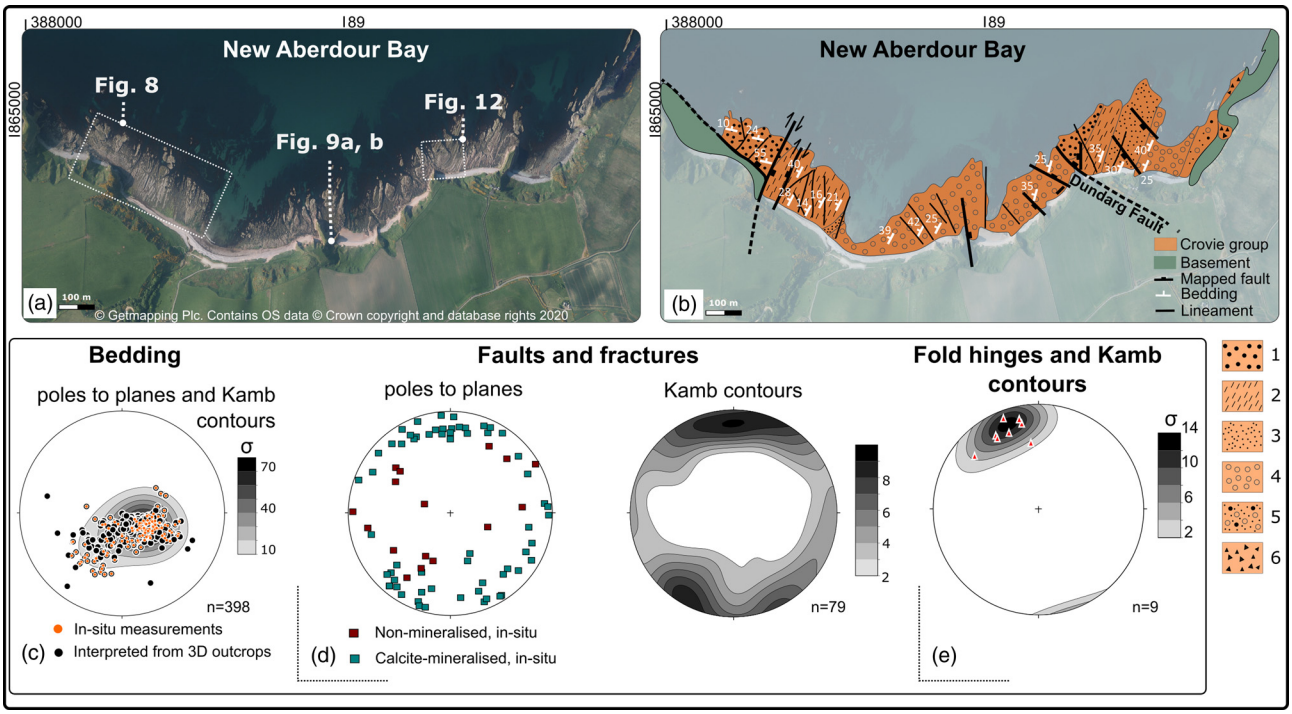

Fig. 7. (**a**) Aerial map (using EdinaDigimap service © Getmapping Plc) and (**b**) geological map of New Aberdour. Lithology data digitized after Sweet (1985); from younger to older: 1, sandstones and siltstones; 2, sandy mudstone, mudstone, limestone; 3, coarse to fine sandstone; 4, conglomeratic sandstone; 5, conglomeratic sandstone with trough cross-bedding; 6, breccia. (**c**–**e**) Stereonets of structural data collected in the field. Lower hemisphere, equal area projections. Locations of Figures 8, 9a, b and 12 are also shown in (**a**).

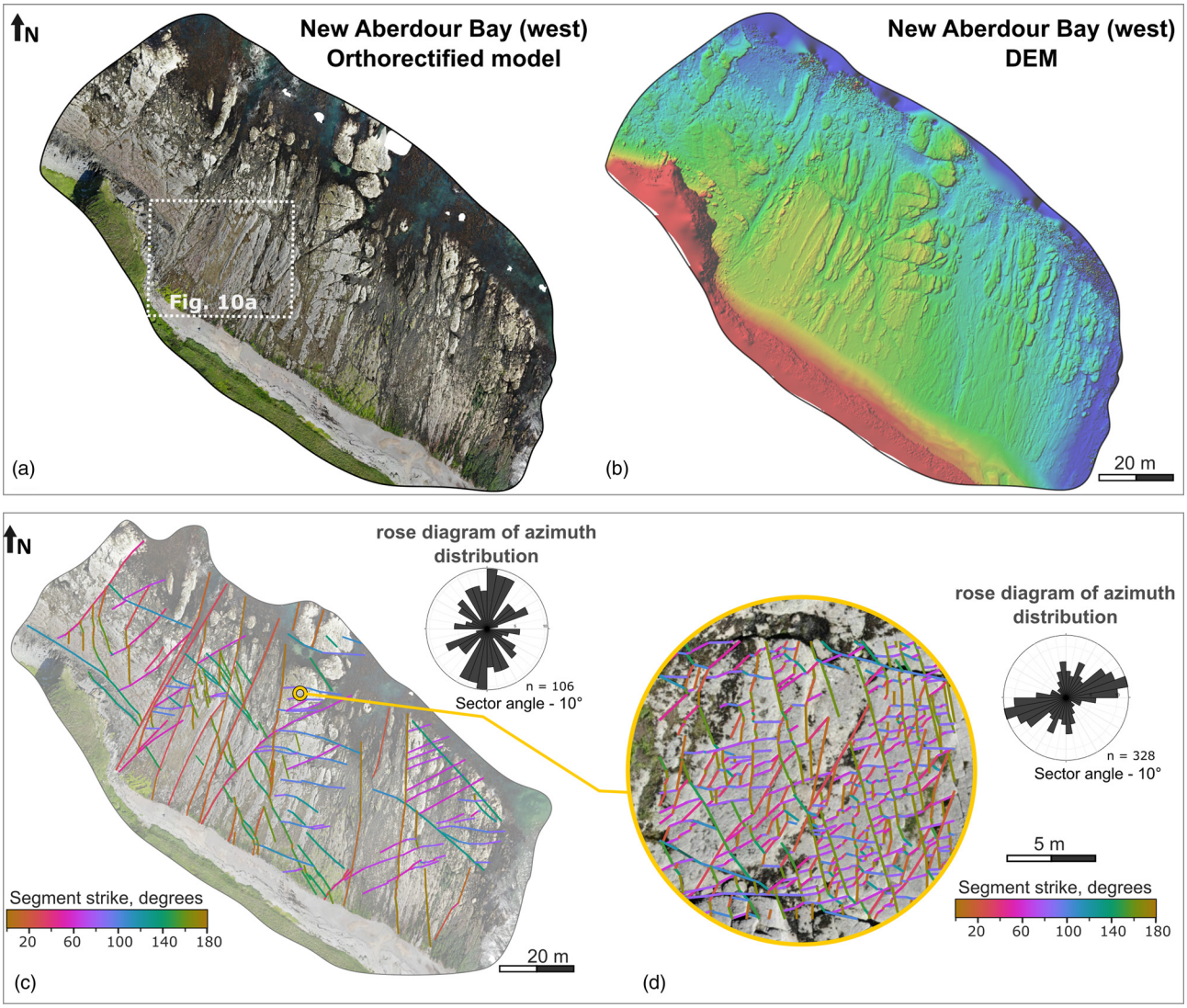

Fig. 8. Overview and lineament interpretation of the western side of New Aberdour Bay. Location of the area shown in Figure 10a is also shown. (**a**) Orthomosaic model obtained from UAV photography. (**b**) DEM, providing high-resolution image for lineament interpretation. Orthomosaic models and inset rose diagram showing lineaments of (**c**) more than *c.* 10 m length and (**d**) less than *c.* 10 m length.

indicate dip-slip normal (Fig. 10c) to slightly sinistral normal, oblique-slip displacements (Fig. 9a).

On the western side of New Aberdour Bay, two intersecting faults, one NNE–SSW-trending (Fault I in Fig. 10a) and the other NW–SE-trending (the latter parallel to a mafic dyke margin), juxtapose the Lower Devonian succession in their hanging walls against the Dalradian basement slates (e.g. Figs 7b and 10a). The NW–SE-trending fault dips steeply towards the NE (dip/dip direction 75°/320°) and poorly preserved slickenlines suggest a normal, sinistral oblique-slip shear sense. The mafic dyke is up to 4 m wide and can be traced for about 150 m to the NW, where it becomes poorly exposed. Other similar subvertical (dipping >85°E) dykes have been observed locally in the Dalradian basement, but none are seen to cross-cut the Devonian succession. This suggests that the dykes most probably predate the Crovie Group and could be Ordovician as suggested for other mafic and ultramafic intrusions in this area (e.g. Read 1923; Gunn *et al.* 2015). Further study is needed to better constrain the nature and age of these dykes.

The NW–SE fault separating basement and cover is crosscut by a steeply east-dipping (80°), calcite-mineralized fault trending NNE–SSW (Fault I, Fig. 10a). This fault has been previously interpreted as a major east-side-down normal fault together with other such faults with this trend in the area (Sweet 1985). Although the exposed fault plane does not preserve kinematic indicators, minor structures present in a 10 m wide damage zone around the fault preserve evidence of shear sense. These include a series of mutually cross-cutting ENE–WSW-trending dextral faults (Fig. 11a), NW–SE sinistral faults and east–west tensile fractures. We interpret these structures as R- and R'-shears and T fractures, respectively, suggesting an overall dextral sense of movement along the main NNE–SSW-trending master fault (Fig. 11d). Other minor dextral north–south- to NNE–SSW-trending faults, parallel to the major fault, have also been observed (Fig. 11c). All of these recorded minor structures are calcite-mineralized. Close to Fault I, drag folding of the Devonian bedding and basement foliation is observed, which is also consistent with dextral movement (Fig. 10a). About 60 m east of Fault I, another major, NNE–SSW-trending fault steeply dipping to the east (74°/290°) occurs (Fault II, Fig. 10a). On the exposed fault plane, both dip-slip slickenline lineations (Fig. 10c) and a later set of normal-dextral calcite slickenfibres (Fig. 10d) are preserved, the latter suggesting that some fault movements have occurred synchronously with carbonate mineralization. Thus the NNE–SSW-trending faults preserve evidence for two episodes of movement: an earlier phase of normal dip-slip and a later set of dextral strike-slip synchronous with calcite mineralization.

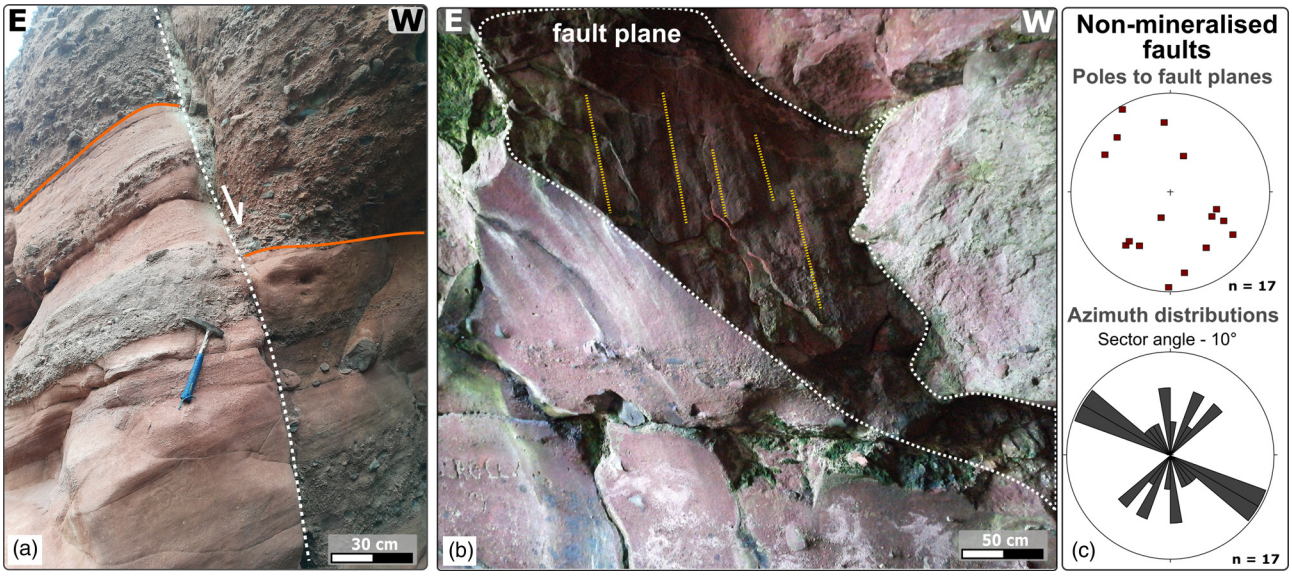

Fig. 9. Example of non-mineralized structures recognized at New Aberdour locality (see location in Fig. 7a). (**a**) Section view of normal fault showing about 50 cm of displacement with minor quantities of green fault gouge. (**b**) Oblique view of clean break fault plane showing dip-slip lineations and grooves. (**c**) Equal area lower hemisphere stereonet and rose plot of non-mineralized faults and fractures at New Aberdour locality.

Folds are commonly visible in the Devonian strata exposed on the flat-lying platform, both on the west and east side of the bay (e.g. Figs 10a and 12a–c). They are usually gentle to open structures (interlimb angles of 120–130°) and plunge shallowly (08–23°) towards the NNW (Fig. 7e). Closer to faults, these folds are tighter (interlimb angles as low as 80°; Fig. 12b) and plunge more steeply (*c.* 40°) towards the north. Extension fractures in the outer arcs of the fold hinge zones are calcite-mineralized (Fig. 10b), suggesting that the folding occurred synchronously with calcite mineralization and the associated faulting episode. Folds are consistently spatially associated with mappable faults (Figs 10b and 12a). Their orientation relative to these north–south to NNE–SSW faults is consistent with dextral kinematics and they have formed synchronous with carbonate mineralization. Away from the faults, bedding is more uniformly dipping to the west (Fig. 7b).

Microscopy

Three representative samples of calcite-mineralized fault zones (S01–03) were selected for microstructural analysis. Sample S01 (Fig. 10d) was collected from the calcite slickenfibres associated with the north–south- to NNE–SSW-trending Fault II (Fig. 10a). Samples S02 (Fig. 11b) and S03 (Fig. 10a) are from minor dextral shear fractures associated with Fault I (Fig. 10a). Further details about the samples are also provided in the Supplementary Material.

All samples show very similar microstructural characteristics (Fig. 13a–f) that are typical of shear veins formed synchronous with fault slip (e.g. see Passchier and Trouw 2005, and references therein). A stacked series of fault-parallel panels with sharp bounding surfaces enclose domains of crystalline and/or fibrous calcite (Fig. 13a and b). The shear veins are either linked together or locally cross-cut by calcite-filled dilational veins that are consistently oriented subparallel to trails of wall rock and fluid inclusions that are best preserved in the fibrous domains (Fig. 13c). The preservation of such inclusion trails is consistent with crack-seal behaviour (Ramsay 1980), and the asymmetry of these trails, the dilational jogs and the fibre obliquity relative to the local fault planes is everywhere consistent with dextral displacements (Fig. 13a, b, d and e). Obliquely oriented tensile calcite veins in sample S02 are closely associated with small gouge-bearing faults in the wall rocks (Fig. 13d and e) which also locally preserve sub-millimetre-spaced Reidel shears consistent with dextral shear (Fig. 13f). Collectively, these textural relationships indicate that calcite mineralization and local right-lateral displacements along north–south- to NNE–SSW-trending faults are contemporaneous.

U–Pb geochronology

The ^{238}U and ^{206}Pb concentrations were analysed in five calcite-bearing samples collected in the field (e.g. Fig. 14a). Samples shown to have approximate concentrations of ^{238}U less than 1 ppb were not analysed any further (three samples; see Supplementary Material), whereas samples with concentrations greater than 1 ppb were mapped in detail using the methods described above. This allowed zones of higher ^{238}U concentration to be identified and targeted for dating. Of the two samples analysed, only one, S02 (Figs 11b and 14a), contained sufficient amounts of ^{238}U (and low enough concentrations of common Pb) to yield an accurate and precise date (it shouldbe noted that LA-ICP-MS data for the unsuccessful sample can be found in the Supplementary Material). For sample S02, 197 spots were ablated, with 68 spots omitted owing to excess common Pb or poor ablation. The remaining spot data (n = 129) were plotted on a Tera–Wasserburg U–Pb plot using IsoplotR (Vermeesch 2018), which yielded a $^{238}U/^{206}Pb$ Model 1 age of 130.99 ± 4.60 Ma (2σ, $Pb_{initial}$ = 0.696 ± 0.0016, MSWD = 0.37; Fig. 14b). The final age uncertainty is fully propagated with reference material uncertainties added in quadrature. It should be noted that a Model 1 age of 131.06 ± 4.48 Ma (2σ, $Pb_{initial}$ = 0.700 ± 0.0013, MSWD = 0.37) is yielded when the excluded data are also plotted (see Supplementary Material). The primary reference material used was WC-1, which yielded a $^{238}U/^{206}Pb$ Model 1 age of 257.22 ± 5.32 Ma (2σ, $Pb_{initial}$ anchored at 0.85, MSWD = 0.13), which is within uncertainty of the expected 255.4 ± 6.4 Ma age reported by Roberts *et al.* (2017). NIST612 was used as a secondary reference material, which yielded isotopic concentrations (^{204}Pb = 38.40 ± 0.92, ^{206}Pb = 38.48 ± 0.15, ^{207}Pb = 38.49 ± 0.21, ^{208}Pb = 38.49 ± 0.31, ^{232}Th = 37.73 ± 0.14, ^{235}U = 37.34 ± 1.29, ^{238}U = 37.16 ± 0.48) within uncertainty of the certified values for NIST612 (38.57 ppm Pb, 37.79 ppm Th and 37.38 ppm U); this was consistently within 2SE of our long-term reproducibility (see Supplementary Material).

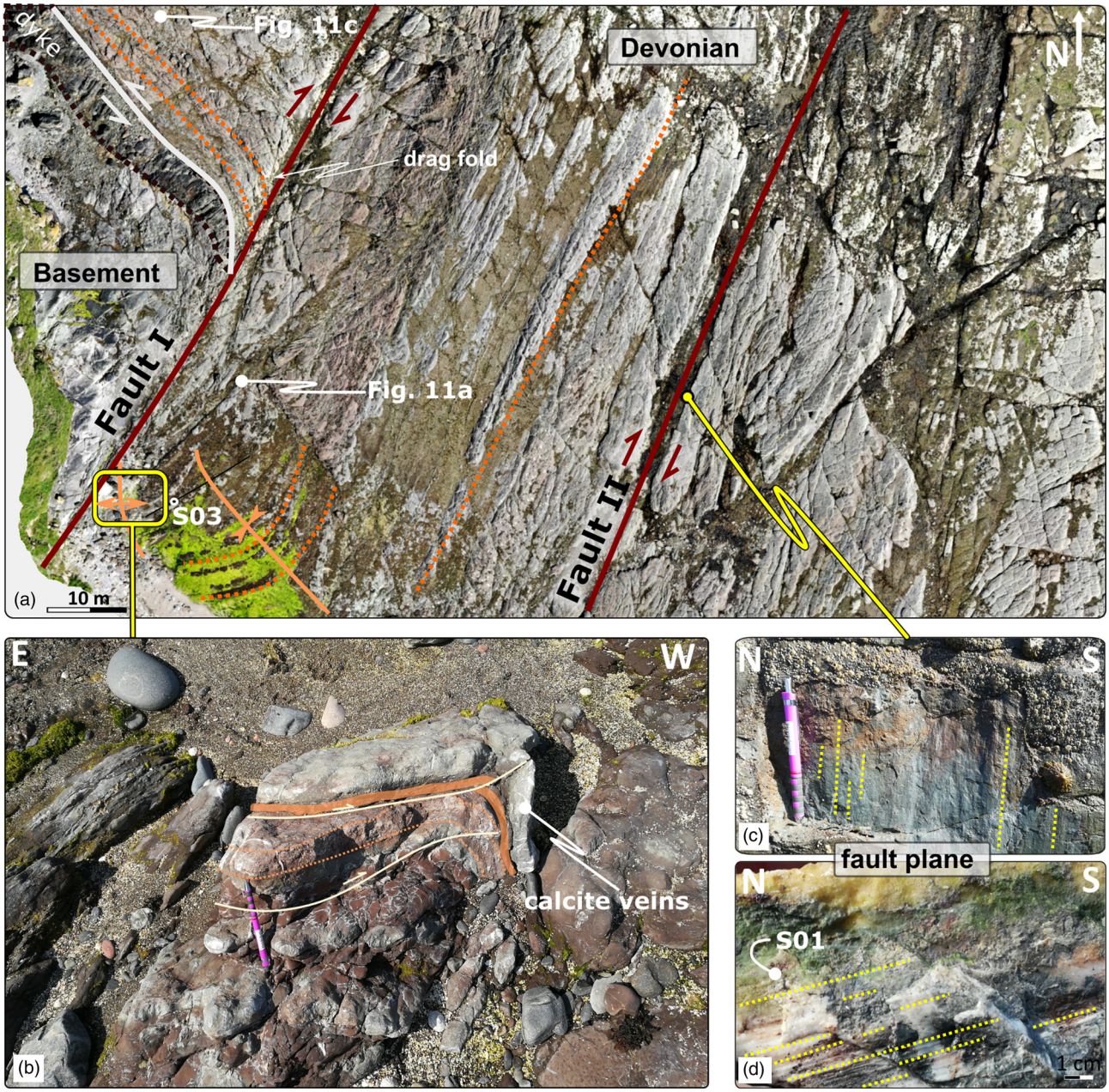

Fig. 10. Examples of faulting and associated structures cross-cutting the Devonian sandstones and Dalradian basement in the western part of the New Aberdour Bay (for location see Fig. 8a). (**a**) Orthomosaic obtained from UAV photography, illustrating dextral reactivated NNE–SSW-striking faults (red) and oblique-sinistral NW–SE-striking faults (white). Bedding and fold axial traces are highlighted in orange. (**b**) NW-plunging tight folds. (**c**) Clean break north–south fault plane showing early dip-slip slickenlines and (**d**) overprinting oblique-dextral calcite slickenfibres with the location of the S01 sample shown.

The low MSWD obtained from the dated carbonate vein sample points to a single isotopic population or mineralization event, despite the isotopic mapping (Fig. 14c) of the sample showing the heterogeneous composition of the precipitated material. The analysed carbonate is enriched in ^{238}U in the vicinity of an incorporated sandstone clast, possibly suggesting leaching of metals from the host rock. Isotopic mapping also reveals a spatial link between the higher ^{238}U and ^{206}Pb concentrations and ^{24}Mg enrichment of the carbonate, with ^{238}U being particularly enriched at the interface between the high and low ^{24}Mg zones (Fig. 14c). Whether this heterogeneity relates to original fluid compositional change or to later alteration or dolomitization is uncertain, although microstructural evidence for later alteration or replacement has not been seen in the samples studied. Heterogeneous ^{24}Mg compositions occur between individual carbonate crystals on the left-hand side of the map with a more uniform ^{24}Mg enrichment towards the right-hand side of the image, which represents the centre of the vein. This suggests that the chemical heterogeneity was a feature of the original carbonate mineralization in the vein, with the Mg (with U and Pb) becoming enriched in the remaining fluid as the vein closed (entraining the wallrock fragment). We therefore tentatively suggest that the chemical variations mapped represent original vein growth processes rather than later alteration, meaning that the $^{238}U/^{206}Pb$ age obtained most probably reflects the time of vein formation and faulting rather than a later fluid flow event.

Main fault types and stress inversion analysis

The north–south- to NNE–SSW-striking normal to slightly sinistral faults are demonstrably synsedimentary based on the growth packages in their hanging walls (Figs 6 and 7a) and are non-mineralized and characterized by clean breaks, fault gouges or

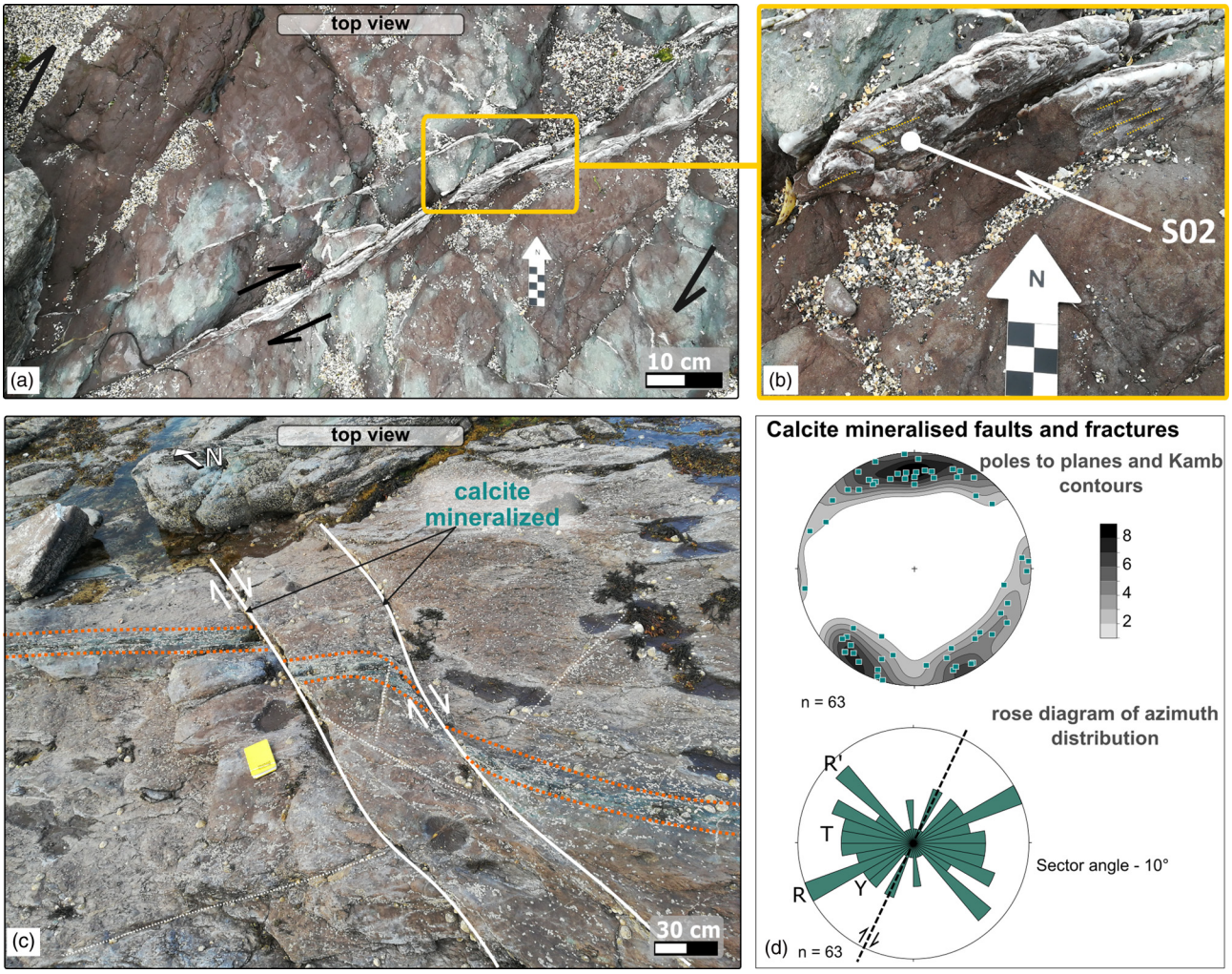

Fig. 11. Examples of calcite-mineralized structures from the New Aberdour locality. (**a**) Plan view of a minor calcite-mineralized dextral fault associated with the major NNE–SSW-trending fault (Fault I in Fig. 10a). (**b**) Close-up of the calcite slickenfibres on the fault plane showing dextral slip with the location of the S02 sample shown. (**c**) Oblique view of other calcite-mineralized north–south- to NNE–SSW-trending dextral faults (white) offsetting bedding (orange). (**d**) Stereonet (lower hemisphere, equal area projection) and rose plot of calcite-mineralized structures.

breccias. Palaeostress inversion analysis of these non-mineralized fault slip data yields an ENE–WSW extension direction (Fig. 15a). The inversion suggests that the faults developed in a regime of near-horizontal extensional stress (σ_3) with an axis oriented 07°/061° and near-vertical compressive stress (σ_1) with an axis oriented 81°/272° (Fig. 15a).

The north–south- to NNE–SSW-striking faults also show evidence of dextral movements (e.g. Fig. 6d), and some preserve evidence of both earlier dip-slip and later dextral-oblique extensional displacement (e.g. Fig. 10c and d). This dextral slip is everywhere associated with calcite mineralization. A palaeostress inversion performed on these calcite-mineralized faults shows that they formed during NNW–SSE rifting (Fig. 15b). The faults were developed in a transtensional regime of horizontal extensional stress (σ_3) with an axis oriented 01°/340° and steeply plunging compressive stress (σ_1) with an axis oriented 67°/247°.

Discussion

Timing and kinematics of faulting

Non-mineralized faulting phase

The NNW–SSE- to NNE–SSW-striking faults characterized by unmineralized clean breaks, fault gouges or breccias were demonstrably established during the Early to Middle Devonian rifting based on the preservation of very well-developed growth packages in their hanging walls (Figs 6 and 7a). Although absolute evidence concerning the age of faulting is not available, it is clear that at least two periods of growth faulting occurred prior to and following the development of the erosional unconformity that separates the supposedly Lower and Middle Devonian sequences. Different fault orientations showing the same fault rock characteristics are interpreted here as being part of the same deformation event. We cannot exclude the possibility that some of the non-mineralized faults are younger, but we have no independent evidence to suggest this. Some could be Permo-Carboniferous structures as suggested by Ashcroft and Wilson (1976), although no faults similar to the Permo-Carboniferous 'Group 2' structures observed in Caithness (as defined by Dichiarante *et al.* 2020) have been identified in our study area. Those structures are typically north–south-trending reverse faults caused by localized inversion of earlier Devonian structures, and are typically associated with north–south-trending folds.

The non-mineralized faults identified in the present study show normal to slightly sinistral-oblique displacements as suggested by the preservation of fault lineations and grooves on exposed slip surfaces (e.g. Fig. 5d and e). Palaeostress inversion analysis of these fault slip data yields an ENE–WSW extension direction (Fig. 15a). These results differ markedly from the NW–SE extension direction suggested by Norton *et al.* (1987), but are

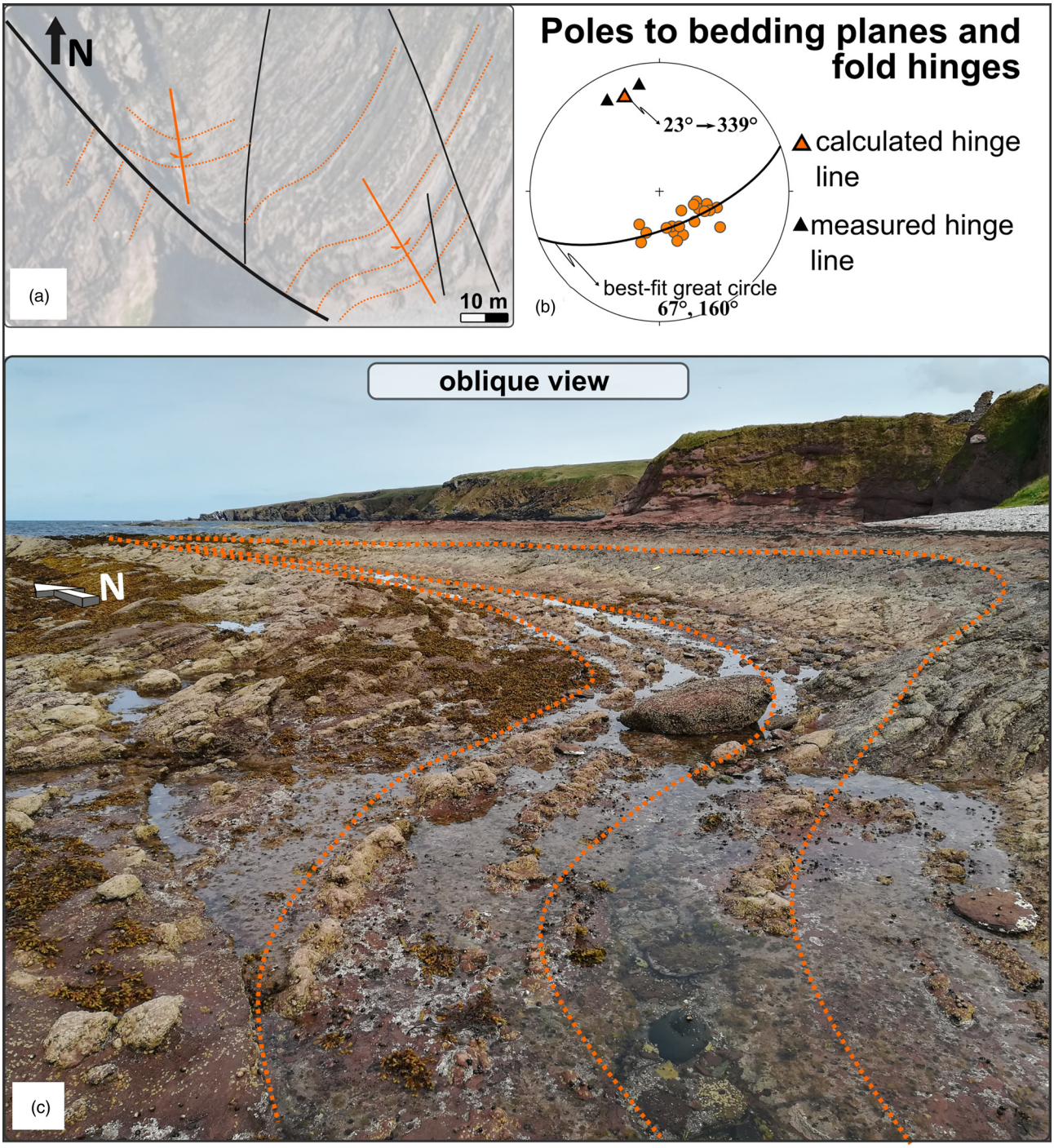

Fig. 12. (**a**) Aerial image and line drawing showing folded strata on the eastern side of the bay. (**b**) Stereonet showing poles to bedding and the hinge lines of the folds. (**c**) Oblique field photograph showing the folded layers looking NE.

comparable with the ENE–WSW extension and similar fault kinematics documented elsewhere in the Orcadian Basin (e.g. Dewey and Strachan 2003; Wilson *et al.* 2010; 'Group 1' structures of Dichiarante *et al.* 2020).

We consider that our results show that the generally north–south-trending faults in the Tariff Sub-basin are related to ENE–WSW sinistral transtensional development of the Orcadian Basin during Devonian left-lateral shear along the Great Glen–Walls Boundary fault system (Seranne 1992; Dewey and Strachan 2003; Watts *et al.* 2007; Wilson *et al.* 2010). This suggests that the regional model for Devonian basin development widely recognized north of the Great Glen Fault can be extended to the southern limits of the Orcadian Basin in the Central Highlands.

Mineralized faulting phase

The Devonian sedimentary rocks are locally cross-cut by a set of younger faults, veins and folds that are associated with widespread syntectonic calcite mineralization (e.g. slickenfibres, tensile veins, Riedel shear fractures, or calcite-cemented fault rocks). Some pre-existing Devonian structures, especially the NNE–SSW-trending faults, experienced oblique-dextral reactivation during this later deformation (e.g. Fig. 10). Stress inversion analyses performed on the calcite-mineralized faults show that they formed during NNW–SSE transtensional deformation (Fig. 15b). NNW-plunging folds are locally developed in proximity to faults, and show calcite-mineralized outer arc extension fractures (Fig. 10b). Although

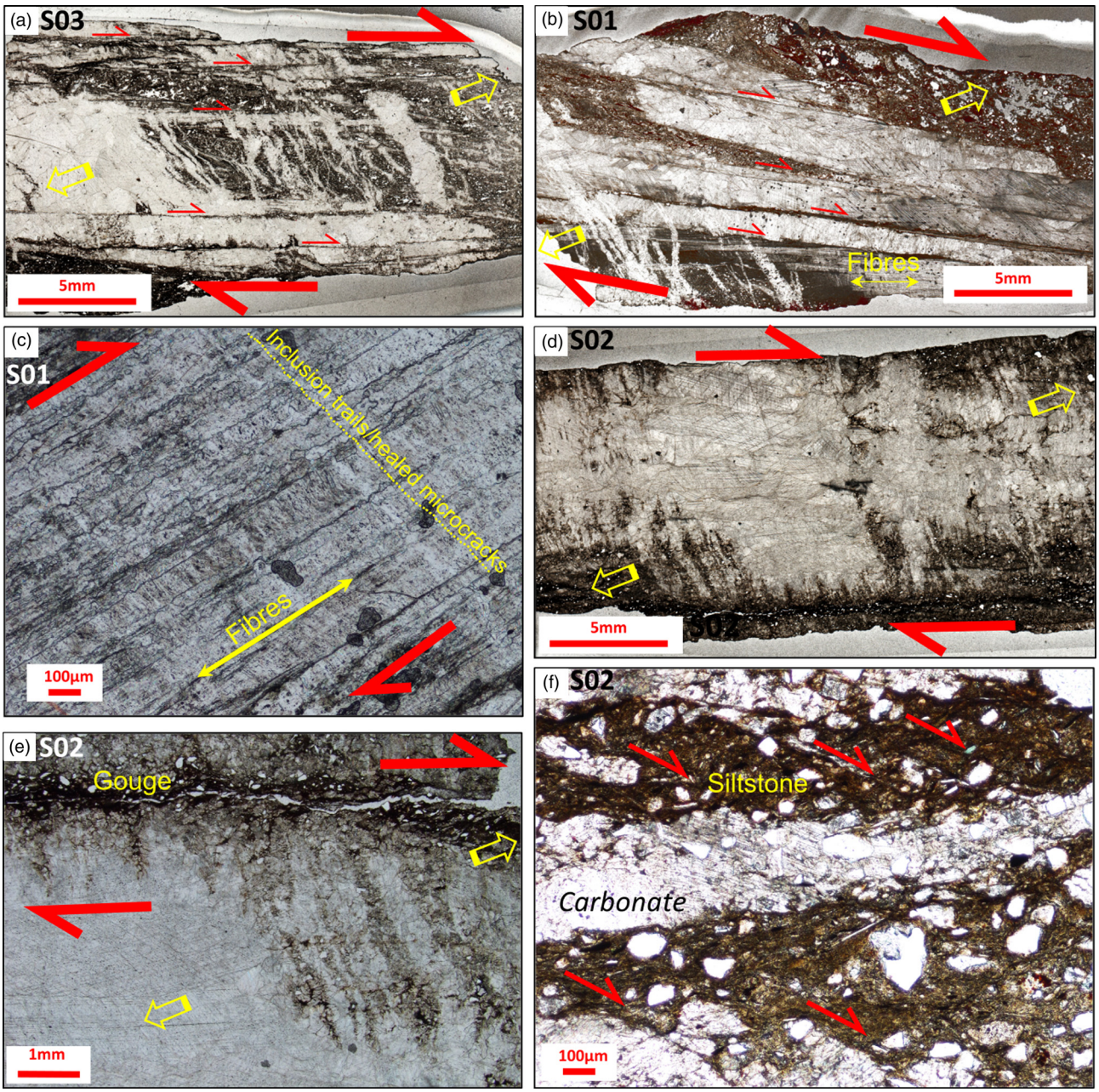

Fig. 13. Photomicrographs of textures associated with calcite-mineralized faults discussed in the text; all images here cut parallel to local slickenline or fibre lineations in the samples and are in plane-polarized light. Red arrows show senses of shear; yellow arrows show local opening and fibre directions. (**a**) and (**b**) Stacked shear and dilational veins in samples S03 and S01, respectively. (Note oblique fibres in (**b**) consistent with dextral shear.) (**c**) High-power view of fibres with aligned crack-seal inclusion trails and healed microfractures (note obliquity consistent with dextral shear). Sample S01. (**d**, **e**) Feathered dilational vein arrays associated with gouge-bearing shear fractures consistent with dextral shear in the dated sample S02. (**f**) Sheared Devonian siltstone and carbonate in dated sample S02 with dextral Riedel/shear bands.

folding seems to be restricted to regions located closer to larger faults, folds developing in an overall transtensional regime are not uncommon (e.g. De Paola *et al.* 2005; Fossen *et al.* 2013). Likewise, the oblique-sinistral NW–SE faults are likely to have been developed during the same event, as their observed kinematics are consistent with the general NNW–SSE transtensional regime.

The new U–Pb dating of the calcite in sample S02, collected from the minor dextral fault (Fig. 11b) interpreted as a synthetic Riedel shear to Fault I, yields an Early Cretaceous age of 130.99 ± 4.60 Ma (Hauterivian) (Fig. 14b). The field evidence (Fig. 11b) and microstructural observations (Fig. 13d–f) suggest strongly that fault displacements were contemporaneous with calcite mineralization. It is therefore proposed that this age also constrains the timing of the younger phase of faulting recognized in the Devonian rocks along the southern coast of the IMFB.

Implications for the regional-scale deformation history of the IMFB

Permo-Triassic

Dextrally reactivated Devonian structures that suggest NW–SE regional rifting have been identified in the northern part of Caithness, where Re–Os geochronology of syntectonic fault-hosted pyrite yielded a Permian age (*c.* 267 Ma) (Dichiarante *et al.* 2016). Although somewhat similar in structural style, on the basis of U–Pb dating, the dextral reactivation of the Devonian structures in our study area is much younger (130.99 ± 4.60 Ma). Furthermore, the Caithness veins are widely associated with base metal sulfides in addition to calcite; such minerals have not been observed along the south coast of the IMFB. Although it is at present unclear whether the Permian deformation in Caithness extends southwards to the NW

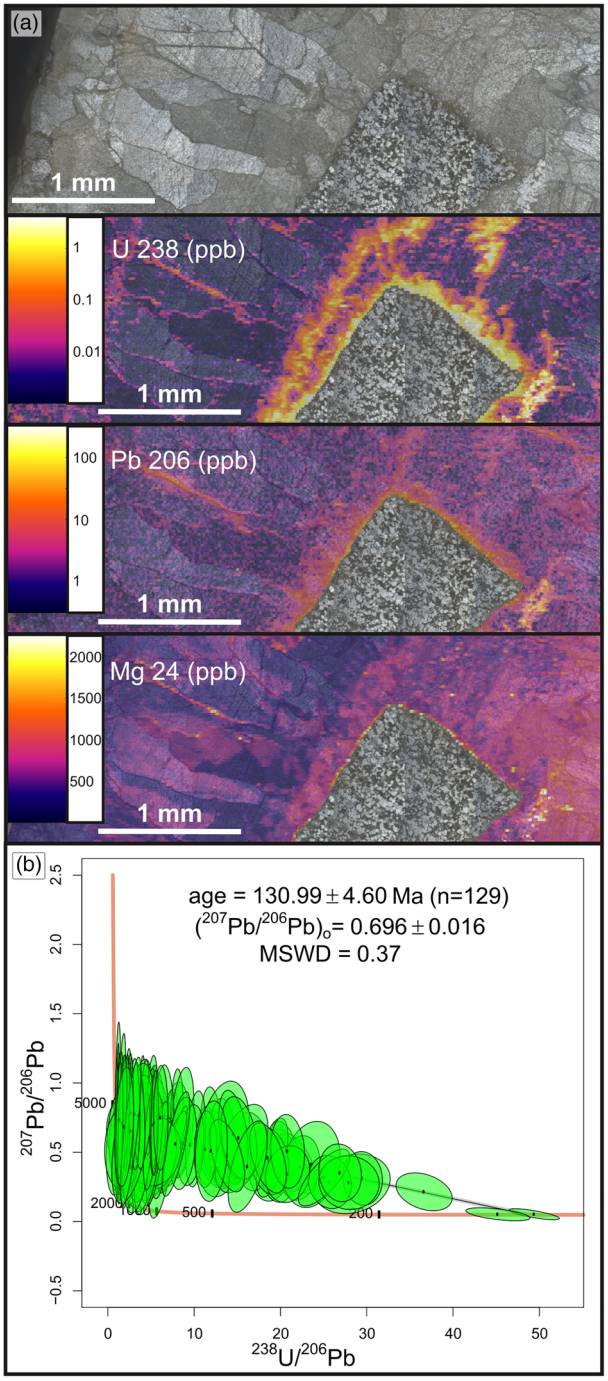

Fig. 14. (**a**) Isotopic concentration maps of ^{238}U, ^{206}Pb and ^{24}Mg generated using LA-ICP-MS trace element mapping in sample S02. (**b**) Tera–Wasserburg diagram of measured *in situ* calcite $^{207}Pb/^{206}Pb$ and $^{238}U/^{206}Pb$ ratios (no common lead correction) from sample S02 (second cycle of the Manndrapselva Member) yielding a Model I discordia age of 130.99 ± 4.60 Ma (2σ, MSWD = 0.37).

flanks of the IMFB, it does not seem to be clearly preserved in the onshore exposures on the south side of the basin. As suggested by Dichiarante *et al.* (2016, 2020), the deformation in Caithness is probably related to the opening of the West Orkney Basin, and may not extend south of the Helmsdale Fault. Hence, the question regarding whether there is onshore evidence for Permo-Triassic deformation in the IMFB remains unresolved.

Late Jurassic–Early Cretaceous

Much of the debate about the relative importance of strike-slip versus dip-slip tectonics in the development of the IMFB came prior to the availability of high-resolution 3D seismic data. More recent models, based on subsurface data of this kind, tend to suggest that there is little evidence for the development of synrift oblique-slip faults in the basin (e.g. Davies *et al.* 2001; Long and Imber 2010; Lăpădat *et al.* 2016). The dextral movement of the Great Glen Fault, which generated oblique- or strike-slip faults in the basin, is widely considered Cenozoic as it also displaces post-rift stratigraphy (e.g. Underhill 1991; Thomson and Underhill 1993; Underhill and Brodie 1993; Davies *et al.* 2001). The Sronlairig Fault, located onshore south of Loch Ness (Fig. 1a), is a ENE–WSW-trending sinistral fault, considered to have developed initially as a synthetic Riedel shear to the sinistral Great Glen Fault during the pre-Late Devonian (428–390 Ma; Stewart *et al.* 1999). Kemp *et al.* (2019) used K–Ar analyses to constrain the timing of the Sronlairig Fault. The results suggest two different times of later fault movement, at 296 ± 7 Ma (Late Carboniferous–Early Permian) and 145 ± 7 Ma (Late Jurassic–Early Cretaceous), respectively. The former event coincides with a widely recognized dextral shearing event along the Great Glen–Wall Boundary fault in northern Scotland, Orkney and Shetland (e.g. see Stewart *et al.* 1999; Armitage *et al.* 2020, and references therein). Kemp *et al.* (2019) suggested that the later age corresponds to the main phase of rifting in the IMFB in the Late Jurassic–Early Cretaceous. They proposed that the Great Glen Fault zone and related structures acted as a northern barrier to active extension at this time, thus explaining the relative absence of deformation at this time in Caithness and the Pentland Firth. Their study further confirms that well-known Caledonian faults onshore may have significant Mesozoic movements and may act as barriers or transfer faults

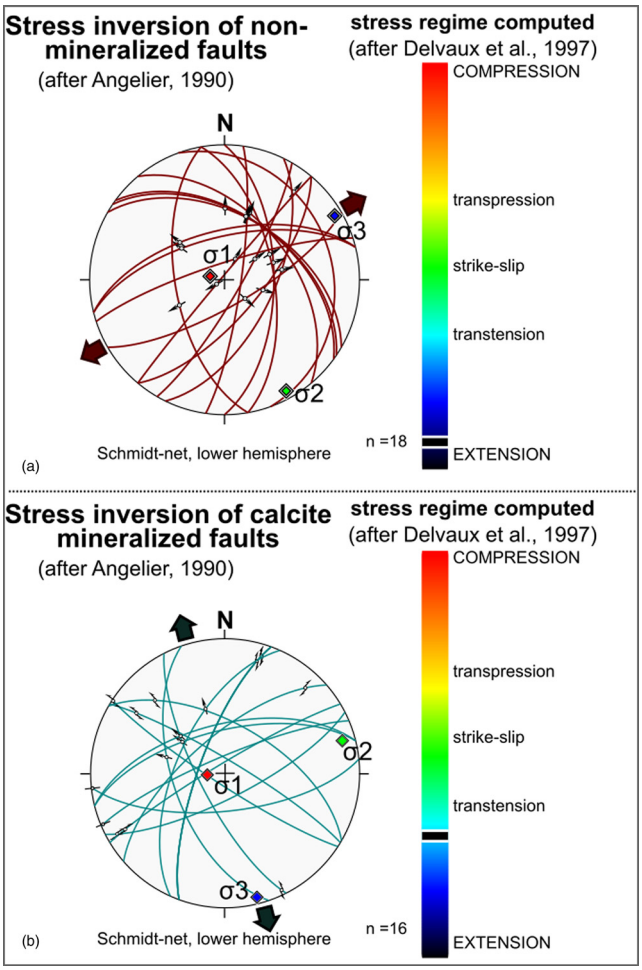

Fig. 15. Stress inversion plots (after Angelier 1990) for (**a**) non-mineralized and (**b**) calcite-mineralized structures.

connecting or bounding younger offshore basins, as originally suggested by Roberts and Holdsworth (1999).

Our findings support the existence of oblique-dextral north–south- to NNE–SSW-trending faults, some of which are proven to have reactivated Devonian structures in the IMFB, during Hauterivian (130.99 ± 4.60 Ma) rifting. This is somewhat later than the Berriasian age previously proposed for the cessation of rifting in offshore areas (e.g. Underhill 1991; Davies *et al.* 2001), but is consistent with studies by Andrews *et al.* (1990), Roberts *et al.* (1990) and Argent *et al.* (2002), all of whom suggested that some faults were longer-lived. The NNW–SSE extension direction deduced from the palaeostress analysis in the present study is parallel to that suggested by Davies *et al.* (2001) based on offshore fault trends, but the timing proposed by them is Late Jurassic (Oxfordian–early Kimmeridgian) rather than Early Cretaceous. During the late Kimmeridgian–Tithonian, they inferred a change to NE–SW extension to explain the development of NW–SW-trending faults in the basin. We suggest that this sequential model should be

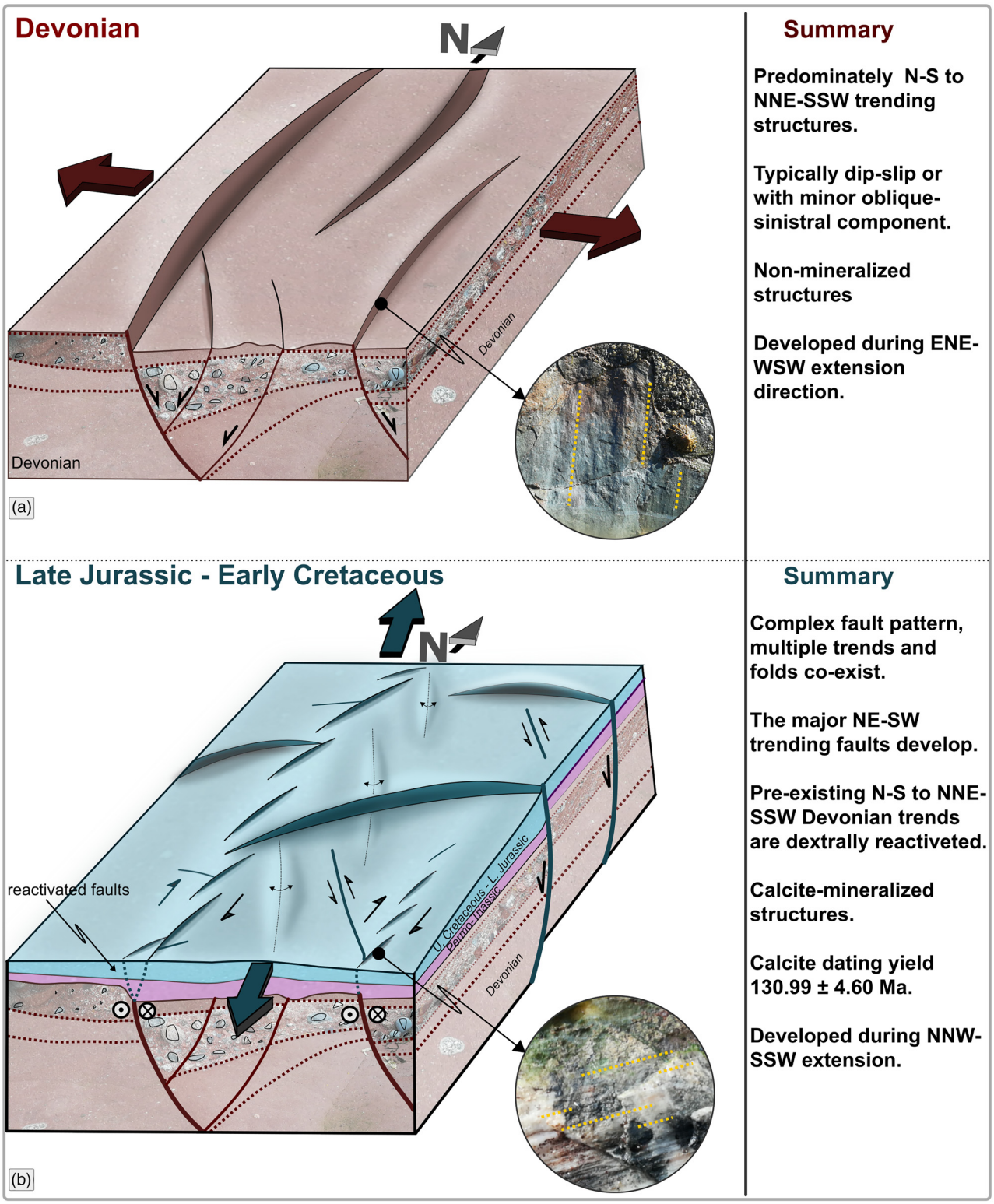

Fig. 16. Summary of the structural history and schematic block diagrams illustrating the superimposed basin development during (**a**) Devonian and (**b**) Late Jurassic–Early Cretaceous.

reassessed and that a synchronous fault development model involving the oblique reactivation of older Orcadian Basin-related structures and the development of new dip-slip faults is also feasible. This would allow multiple fault families to coexist, including the main basin- to sub-basin-bounding NE–SW dip-slip normal faults, in addition to smaller scale transtensional dextral north–south to NNE–SSW faults, sinistral NW–SE faults and local folds. Oblique kinematics and reactivation of pre-existing structures have certainly been identified elsewhere in the North Sea (e.g. Færseth *et al.* 1997). More generally, this model is consistent with the suggestion that simple orthogonal rifting models are less common than is generally assumed (e.g. Holdsworth *et al.* 1997; Dewey *et al.* 1998; Dichiarante *et al.* 2020). Further integration of high-resolution offshore 3D seismic reflection data should be used to confirm whether the trends observed onshore in the Turniff Sub-basin can be recognized offshore in the IMFB.

Implications for prospectivity of Devonian-involved plays

In the IMFB, the main reservoir-seal packages are thought to comprise Lower Jurassic to Middle Jurassic sandstones and siltstones interbedded with mudstones. The Beatrice field (Linsley *et al.* 1980; Fig. 1b), which was the most significant field in the region, is considered to have been charged by a combination of Devonian and Jurassic source rocks (e.g. Peters *et al.* 1989; Greenhalgh 2016). The Devonian source rock in the offshore IMFB is largely thought to lie in the oil window and co-sources other fields in the Orcadian Basin (e.g. Greenhalgh 2016). Fractured Devonian sandstones provide known local petroleum reservoirs elsewhere in the North Sea (e.g. Claymore, Buchan, Stirling fields; Marshall and Hewett 2003). Also, the Clair field, west of Shetland, is a giant oilfield hosted in fractured Carboniferous–Devonian and Precambrian basement rocks, with a Kimmeridge Clay source (Coney *et al.* 1993; Holdsworth *et al.* 2019). The development of reservoir-quality fractured sandstones and local Devonian source rocks in the oil window provide evidence that this type of play could be more extensive. Oil-stained Devonian and basement rocks have certainly been identified in many locations onshore Moray Firth (Greenhalgh 2016, and references therein) and are also locally observed in the highly fractured sandstones at Pennan (Fig. 5d and e).

Our findings show that the Devonian rocks underwent both Devonian and Early Cretaceous deformation, with oblique reactivation of Devonian structures during the later stage. This led to a high density of faults and fracture networks (e.g. Fig. 8c and d), which are critical for the development of potential Devonian-involved plays. Although there are some similarities in terms of structural style, the reactivation events recognized in the southern part of the former Orcadian Basin are significantly younger than those recognized further to the north (e.g. Caithness, West Orkney Basin).

Conclusions

Our integrated onshore study combines structural studies with absolute U–Pb calcite dating techniques to reveal two main deformation events in the southern part of the superimposed Inner Moray Firth and Orcadian basins.

The earliest event is demonstrably Devonian based on the preservation of growth faulting (Fig. 16a) and is characterized by the development of dip-slip to oblique-sinistral, non-mineralized faults predominantly striking north–south to NNE–SSW. Palaeostress inversion analyses suggest that they developed during ENE–WSW extension and are related to the opening of the Orcadian Basin during sinistral transtensional displacements along the Great Glen Fault. This suggests that the regional tectonic model recognized in the northern part of the Orcadian Basin (e.g. Wilson *et al.* 2010; Dichiarante *et al.* 2020) can be extended southwards into the Central Highlands. It is also kinematically compatible with transtensional rifting and strike-slip tectonics on the Midland Valley at this time (e.g. Dewey and Strachan 2003).

These early formed Devonian structures show evidence of later dextral reactivation during a widespread phase of NNW–SSE extension. Also, NE–SW- to WNW–ESE- and NW–SE-striking faults (showing oblique-sinistral kinematics) and NNW-plunging folds formed at the same time (Fig. 16b). This later deformation is consistently associated with syntectonic calcite mineralization (e.g. shear veins, slickenfibres, tensile veins and Riedel shears). U–Pb calcite dating suggests that the timing of faulting and fault reactivation of pre-existing Devonian structures associated with calcite mineralization is Early Cretaceous (130.99 ± 4.60 Ma). We consider this to have occurred during the latter stages of the more regionally recognized Late Jurassic to Early Cretaceous opening of the IMFB (Davies *et al.* 2001; Argent *et al.* 2002). This provides the first clear evidence that strike-slip and oblique-slip faults coexist in the IMFB during the basin opening. It also provides clear evidence that the main rift-related deformation extends beyond the Banff Fault in the southern part of the IMFB, and into the onshore Turriff Sub-basin, even though younger stratigraphy is not preserved here.

To explain the different fault orientations associated with the Late Jurassic–Early Cretaceous deformation, we favour synchronous development of these structures during transtension and fault reactivation, rather than in-sequence faulting owing to stress rotation at different times (as suggested by Davies *et al.* 2001, for example). Complex fault patterns have been widely associated with transtension and oblique rifting (e.g. Wilson *et al.* 2006, 2010) and we believe this is the case, at least locally, in the IMFB. Thus, oblique reactivation of pre-existing faults during later rifting episodes leads to the development of highly localized regions of complex deformation that contrast strongly with intervening regions of relatively undeformed, shallowly dipping strata. The scale and kinematics of these structures are directly controlled by the location, scale and orientation of the older inherited faults at depth.

The integration of fieldwork, stress inversion analyses and absolute dating techniques shows that widespread oblique reactivation of earlier Orcadian Basin structures has occurred. This will create reservoir-scale structural heterogeneity in potential Devonian reservoirs and can be used to further explore subsurface Devonian-involved plays elsewhere in the North Sea.

Acknowledgements This research is based on the PhD work of A.T. undertaken as part of the Natural Environment Research Council (NERC) Centre for Doctoral Training (CDT) in Oil and Gas (grant number NEM00578X/1) and was funded by Durham University and British Geological Survey (BGS) via the British University Funding Initiative (BUFI), whose support is gratefully acknowledged. We acknowledge the provision of very thorough review comments by C. Mottram and G. Leslie. I. Chaplin is thanked for his outstanding thin-section preparation. The authors are also grateful to J. Lee and N. Roberts (BGS geochronology lab) for attempting calcite dating of some of our samples, which unfortunately gave no viable age data. N. Roberts is also thanked for his constructive comments on geochronology. D.M. contributes here by permission of the Executive Director, British Geological Survey, UKRI.

Author contributions **AT**: conceptualization (lead), data curation (lead), formal analysis (lead), investigation (lead), methodology (lead), software (equal), visualization (lead), writing – original draft (lead); **REH**: conceptualization (supporting), data curation (supporting), formal analysis (supporting), funding acquisition (equal), investigation (supporting), methodology (equal), supervision (equal), validation (lead), writing – original draft (supporting), writing – review & editing (lead); **JRU**: conceptualization (supporting), data curation (supporting), funding acquisition (equal), supervision (equal), validation (supporting), writing – review & editing (supporting); **DMT**: data curation (supporting), investigation (supporting), methodology (equal), software (equal), visualization (supporting), writing – original draft (supporting), writing – review & editing (supporting); **EDD**: investigation (supporting), methodology (equal),

visualization (supporting), writing – original draft (supporting), writing – review & editing (supporting); **KH**: investigation (supporting), methodology (supporting), writing – review & editing (supporting); **AB**: investigation (supporting), methodology (supporting), writing – review & editing (supporting); **DM**: supervision (supporting), validation (supporting), writing – review & editing (supporting); **KJWM**: supervision (supporting), validation (supporting), writing – review & editing (supporting); **DS**: supervision (supporting), validation (supporting), writing – review & editing (supporting)

Funding This work was funded by the Durham University, British Geological Survey and Natural Environment Research Council.

Data availability All data generated or analysed during this study are included in this published article (and its supplementary information files).

Scientific editing by John MacDonald

References

Allmendinger, R.W., Cardozo, N. and Fisher, D. 2012. *Structural Geology Algorithms: Vectors and Tensors in Structural Geology*. Cambridge University Press, Cambridge.

Andrews, I.J., Long, D., Richards, P.C., Thomson, A.R., Brown, S., Chesher, J.A. and McCormac, M. 1990. *The Geology of the Moray Firth*. HMSO, London.

Angelier, J. 1984. Tectonic analysis of fault slip data sets. *Journal of Geophysical Research*, **89**, 5835–5848, https://doi.org/10.1029/JB089iB07p05835

Angelier, J. 1990. Inversion of field data in fault tectonics to obtain the regional stress III: a new rapid direct inversion method by analytical means. *Geophysical Journal International*, **103**, 363–376, https://doi.org/10.1111/j.1365-246X.1990.tb01777.x

Argent, J., Stewart, S.A., Green, P. and Underhill, J.R. 2002. Heterogeneous exhumation in the Inner Moray Firth, UK North Sea: constraints from new AFTA® and seismic data. *Journal of the Geological Society, London*, **159**, 715–729, https://doi.org/10.1144/0016-764901-141

Armitage, T.B., Watts, L.M., Holdsworth, R.E. and Strachan, R.A. 2020. Late Carboniferous dextral transpressional reactivation of the crustal-scale Walls Boundary Fault, Shetland: the role of pre-existing structures and lithological heterogeneities. *Journal of the Geological Society, London*, **178**, jgs2020-078, https://doi.org/10.1144/jgs2020-078

Ashcroft, W.A. and Wilson, C.D.V. 1976. A geophysical survey of the Turriff basin of Old Red Sandstone, Aberdeenshire. *Journal of the Geological Society, London*, **132**, 27–43, https://doi.org/10.1144/gsjgs.132.1.0027

Bell, R.E., Jackson, C.A.-L., Whipp, P.S. and Clements, B. 2014. Strain migration during multiphase extension: observations from the northern North Sea. *Tectonics*, **33**, 1936–1963, https://doi.org/10.1002/2014TC003551

Bird, T.J., Bell, A., Gibbs, A.D. and Nicholson, J. 1987. Aspects of strike-slip tectonics in the Inner Moray Firth Basin, offshore Scotland. *Norsk Geologisk Tidsskrift*, **67**, 353–369.

Bott, M. 1959. The mechanics of oblique slip faulting. *Geological Magazine*, **96**, 109–117, https://doi.org/10.1017/S0016756800059987

Brewer, J.A. and Smythe, D.K. 1984. MOIST and the continuity of crustal reflector geometry along the Caledonian–Appalachian orogen. *Journal of the Geological Society, London*, **141**, 105–120, https://doi.org/10.1144/gsjgs.141.1.0105

BGS. 1987. *Fraserburgh, Sheet 97. 1:50 000*. Ordnance Survey, Southampton.

BGS. 1995. *BGS Moray Firth (Special Sheet), 1:250 000*. British Geological Survey, Edinburgh.

Buchan, S. 1932. On some dykes in east Aberdeenshire. *Transactions of the Edinburgh Geological Society*, **12**, 323–328, https://doi.org/10.1144/transed.12.4.323

Cardozo, N. and Allmendinger, R.W. 2013, Spherical projections with OSXStereonet. *Computers & Geosciences*, **51**, 193–205, https://doi.org/10.1016/j.cageo.2012.07.021

Coney, D., Fyfe, T.B., Retail, P. and Smith, P.J. 1993. Clair Appraisal – the benefits of a co-operative approach. *Geological Society, London, Petroleum Geology Conference Series*, **4**, 1409–1420, https://doi.org/10.1144/0041409

Coward, M.P. and Enfield, M.A. 1987. The structure of the West Orkneys and associated basins. *In*: Brooks, J. amd Glennie, K.W. (eds) Petroleum Geology of North West Europe. Proceedings of the Third Conference on Petroleum Geology of North West Europe. Graham & Trotman, London, 687–696.

Coward, M.P., Enfield, M.A. and Fischer, M.W. 1989. Devonian basins of Northern Scotland: extension and inversion related to Late Caledonian–Variscan tectonics. *Geological Society, London, Special Publications*, **44**, 275–308, https://doi.org/10.1144/GSL.SP.1989.044.01.16

Davies, R.J., Turner, J.D. and Underhill, J.R. 2001. Sequential dip-slip fault movement during rifting: a new model for the evolution of the Jurassic trilete North Sea rift system. *Petroleum Geoscience*, **7**, 371–388, https://doi.org/10.1144/petgeo.7.4.371

Delvaux, D., Moeys, R. *et al.* 1997. Paleostress reconstructions and geodynamics of the Baikal region, Central Asia, Part 2. Cenozoic rifting. *Tectonophysics*, **282**, 1–38, https://doi.org/10.1016/S0040-1951(97)00210-2

De Paola, N., Holdsworth, R.E., McCaffrey, K.J.W. and Barchi, M.R. 2005. Partitioned transtension: an alternative to basin inversion models. *Journal of Structural Geology*, **27**, 607–625, https://doi.org/10.1016/j.jsg.2005.01.006

Dewey, J.F. and Strachan, R.A. 2003. Changing Silurian–Devonian relative plate motion in the Caledonides: sinistral transpression to sinistral transtension. *Journal of the Geological Society, London*, **160**, 219–229, https://doi.org/10.1144/0016-764902-085

Dewey, J.F., Holdsworth, R.E. and Strachan, R.A. 1998. Transpression and transtension zones. *Geological Society, London, Special Publications*, **135**, 1–14, https://doi.org/10.1144/GSL.SP.1998.135.01.01

Dichiarante, A.M., Holdsworth, R.E. *et al.* 2016. New structural and Re–Os geochronological evidence constraining the age of faulting and associated mineralization in the Devonian Orcadian Basin, Scotland. *Journal of the Geological Society, London*, **173**, 457–473, https://doi.org/10.1144/jgs2015-118

Dichiarante, A.M., Holdsworth, R.E., Dempsey, E.D., McCaffrey, K.J.W. and Utley, T.A.G. 2020. Outcrop-scale manifestations of reactivation during multiple superimposed rifting and basin inversion events: the Devonian Orcadian Basin, northern Scotland. *Journal of the Geological Society, London*, **178**, jgs2020-089, https://doi.org/10.1144/jgs2020-089

Duncan, W.I. and Buxton, N.W.K. 1995. New evidence for evaporitic Middle Devonian lacustrine sediments with hydrocarbon source potential on the East Shetland Platform, North Sea. *Journal of the Geological Society, London*, **152**, 251–258, https://doi.org/10.1144/gsjgs.152.2.0251

Enfield, M.A. and Coward, M.P. 1987. The Structure of the West Orkney Basin, northern Scotland. *Journal of the Geological Society, London*, **144**, 871–884, https://doi.org/10.1144/gsjgs.144.6.0871

Færseth, R.B., Knudsen, B.-E., Liljedahl, T., Midbøe, P.S. and Søderstrøm, B. 1997. Oblique rifting and sequential faulting in the Jurassic development of the northern North Sea. *Journal of Structural Geology*, **19**, 1285–1302, https://doi.org/10.1016/S0191-8141(97)00045-X

Fazlikhani, H., Aagotnes, S.S. *et al.* 2020. Strain migration during multiphase extension, Stord Basin, northern North Sea rift. *Basin Research*, **33**, 1474–1496, https://doi.org/10.1111/bre.12522

Fossen, H., Teyssier, C. and Whitney, D.L. 2013. Transtensional folding. *Journal of Structural Geology*, **56**, 89–102, https://doi.org/10.1016/j.jsg.2013.09.004

Fournier, M., Bellahsen, N., Fabbri, O. and Gunnell, Y. 2004. Oblique rifting and segmentation of the NE Gulf of Aden passive margin. *Geochemistry, Geophysics, Geosystems*, **5**, Q11005, https://doi.org/10.1029/2004GC000731

Friend, P.F., Williams, B.J., Ford, M. and Williams, E.A. 2000. Kinematics and dynamics of Old Red Sandstone basins. *Geological Society, London, Special Publications*, **180**, 29–60, https://doi.org/10.1144/GSL.SP.2000.180.01.04

Frostick, L., Reid, I., Jarvis, J. and Eardley, H. 1988. Triassic sediments of the Inner Moray Firth, Scotland: early rift deposits. *Journal of the Geological Society, London*, **145**, 235–248, https://doi.org/10.1144/gsjgs.145.2.0235

Greenhalgh, E. 2016. *Literature Review of Devonian Source Rocks and Devonian-Sourced Hydrocarbons in the Orcadian Basin*. British Geological Survey Commissioned Report, **CR/16/017**.

Guariguata-Rojas, G.J. and Underhill, J.R. 2017. Implications of Early Cenozoic uplift and fault reactivation for carbon storage in the Moray Firth Basin. *Interpretation*, **5**, SS1–SS21, https://doi.org/10.1190/INT-2017-0009.1

Gunn, A.G., Mendum, J.R. and Thomas, C.W. 2015. *Geology of the Huntly and Turriff Districts. Sheet Description for the 1:50 000 Geological Sheets 86W (Huntly) and 86E (Turriff)*. British Geological Survey, Edinburgh.

Hansen, J.-A., Bergh, S.G. and Henningsen, T. 2012. Mesozoic rifting and basin evolution on the Lofoten and Vesterålen Margin, North-Norway; time constraints and regional implications. *Norwegian Journal of Geology*, **91**, 203–228, https://doi.org/10.1111/bre.12358

Healy, D., Rizzo, R.E. *et al.* 2017. Fracpaq: a MATLAB toolbox for the quantification of fracture patterns. *Journal of Structural Geology*, **95**, 1–16, https://doi.org/10.1016/j.jsg.2016.12.003

Henstra, G.A., Berg Kristensen, T., Rotevatn, A. and Gawthorpe, R.L. 2019. How do pre-existing normal faults influence rift geometry? A comparison of adjacent basins with contrasting underlying structure on the Lofoten Margin, Norway. *Basin Research*, **31**, 1083–1097, https://doi.org/10.1111/bre.12358

Hoareau, G., Claverie, F. *et al.* 2020. Direct U–Pb dating of carbonates from micron scale femtosecond laser ablation inductively coupled plasma mass spectrometry images using robust regression. *Geochronology Discussion*, **3**, 67–87, https://doi.org/10.5194/gchron-3-67-2021

Hodgetts, D., Gawthorpe, R.L., Wilson, P. and Rarity, F. 2007. Integrating digital and traditional field techniques using virtual reality geological studio (VRGS). 69th European Association of Geoscientists and Engineers Conference and Exhibition 2007, Securing the Future. Society of Petroleum Engineers, London, UK, 83–87.

Holdsworth, R.E., Butler, C.A. and Roberts, A.M. 1997. The recognition of reactivation during continental deformation. *Journal of the Geological Society, London*, **154**, 73–78, https://doi.org/10.1144/gsjgs.154.1.0073

Holdsworth, R.E., McCaffrey, K.J.W. *et al.* 2019. Natural fracture propping and earthquake-induced oil migration in fractured basement reservoirs. *Geology*, **47**, 700–704, https://doi.org/10.1130/G46280.1

Holdsworth, R.E., Trice, R. *et al.* 2020. The nature and age of basement host rocks and fissure fills in the Lancaster field fractured reservoir, West of Shetland. *Journal of the Geological Society, London*, **177**, 1057–1073, https://doi.org/10.1144/jgs2019-142

Hurst, A.R. 1981. Mid Jurassic stratigraphy and facies at Brora, Sutherland. *Scottish Journal of Geology*, **17**, 169–177, https://doi.org/10.1144/sjg17030169
Johnstone, G.S. and Mykura, W. 1989. *British Regional Geology: the Northern Highlands of Scotland*, **2**. HMSO, London.
Kamb, W.B. 1959. Ice petrofabric observations from Blue Glacier, Washington, in relation to theory and experiment. *Journal of Geophysical Research*, **64**, 1891–1909, https://doi.org/10.1029/JZ064i011p01891
Kemp, S., Gillespie, M., Leslie, G., Zwingmann, H. and Campbell, S. 2019. Clay mineral dating of displacement on the Sronlairig Fault: implications for Mesozoic and Cenozoic tectonic evolution in northern Scotland. *Clay Minerals*, **54**, 181–196, https://doi.org/10.1180/clm.2019.25
Kylander-Clark, A.R. 2020. Expanding the limits of laser-ablation U–Pb calcite geochronology. *Geochronology*, **2**, 343–354, https://doi.org/10.5194/gchron-2-343-2020
Lăpădat, A., Imber, J., Yielding, G., Iacopini, D., McCaffrey, K.J.W., Long, J.J. and Jones, R.R. 2016. Occurrence and development of folding related to normal faulting within a mechanically heterogeneous sedimentary sequence: a case study from Inner Moray Firth, UK. *Geological Society, London, Special Publications*, **439**, 373–394, https://doi.org/10.1144/SP439.18
Le Breton, E., Cobbold, P.R. and Zanella, A. 2013. Cenozoic reactivation of the Great Glen Fault, Scotland: additional evidence and possible causes. *Journal of the Geological Society, London*, **170**, 403–415, https://doi.org/10.1144/jgs2012-067
Linsley, P.N., Potter, H.C., Mcnab, G. and Racher, D. 1980. The Beatrice field, Inner Moray Firth, U.K. North Sea. *AAPG Memoirs*, **30**, 117–129.
Long, J.J. and Imber, J. 2010. Geometrically coherent continuous deformation in the volume surrounding a seismically imaged normal fault-array. *Journal of Structural Geology*, **32**, 222–234, https://doi.org/10.1016/j.jsg.2009.11.009
Lovecchio, J.P., Rohais, S., Joseph, P, Bolatti, N.D., Kress, P.R., Gerster, R. and Ramos, V.A. 2018. Multistage rifting evolution of the Colorado basin (offshore Argentina): evidence for extensional settings prior to the South Atlantic opening. *Terra Nova*, **30**, 359–368, https://doi.org/10.1111/ter.12351
Macgregor, D. 2015 History of the development of the East African Rift System: a series of interpreted maps through time. *Journal of African Earth Sciences*, **101**, 232–252, https://doi.org/10.1016/j.jafrearsci.2014.09.016
Marshall, J.E.A. and Hewett, A.J. 2003. Devonian. *In*: Evans, D., Graham, C., Armour, A. and Bathurst, P. (eds) *Millennium Atlas: Petroleum Geology of the Northern North Sea*. Geological Society, London, 64–81.
McArthur, A.D., Hartley, A.J. and Jolley, D.W. 2013. Stratigraphic development of an Upper Jurassic deep marine syn-rift succession, Inner Moray Firth Basin, Scotland. *Basin Research*, **25**, 285–309, https://doi.org/10.1111/j.1365-2117.2012.00557.x
McCaffrey, K.J.W., Jones, R.R. *et al.* 2005. Unlocking the spatial dimension: digital technologies and the future of geoscience fieldwork. *Journal of the Geological Society, London*, **162**, 927–938, https://doi.org/10.1144/0016-764905-017
McClay, K., Norton, M.G. *et al.* 1986. Collapse of the Caledonian orogen and the Old Red Sandstone. *Nature*, **323**, 147–149, https://doi.org/10.1038/323147a0
McQuillin, R., Donato, J.A. and Tulstrup, J. 1982. Development of basins in the Inner Moray Firth and the North Sea by crustal extension and dextral displacement of the Great Glen Fault. *Earth and Planetary Science Letters*, **60**, 127–139, https://doi.org/10.1016/0012-821X(82)90028-0
Michael, A.J. 1984. Determination of stress from slip data: faults and folds. *Journal of Geophysical Research: Solid Earth*, **89**, 11517–11526, https://doi.org/10.1029/JB089iB13p11517
Mostafa, M.E. 2005. Iterative direct inversion: an exact complementary solution for inverting fault-slip data to obtain palaeostresses. *Computers & Geosciences*, **31**, 1059–1070, https://doi.org/10.1016/j.cageo.2005.02.012
NIREX 1994. *The Geology of the Region Around Dounreay: Report of the Regional Geology Joint Interpretation Team*. UK Nirex Limited Report, **657**.
Norton, M.J., McClay, K.R. and Nick, A.W. 1987. Tectonic evolution of Devonian basins in northern Scotland and southern Norway. *Norsk Geologisk Tidsskrift*, **67**, 323.
Passchier, C. and Trouw, R. 2005. *Microtectonics*. Springer, Berlin.
Peters, K.E., Moldowan, J.M., Driscole, A.R. and Demaison, G.J. 1989. Origin of Beatrice Oil by Co-Sourcing from Devonian and Middle Jurassic Source Rocks, Inner Moray Firth, United Kingdom. *AAPG Bulletin*, **73**, 454–471, https://doi.org/10.1306/44B49FCE-170A-11D7-8645000102C1865D
Petit, J.P. 1987. Criteria for the sense of movement on fault surfaces in brittle rocks. *Journal of Structural Geology*, **9**, 597–608, https://doi.org/10.1016/0191-8141(87)90145-3
Pickering, K.T. 1984. The Upper Jurassic 'Boulder Beds' and related deposits: a fault-controlled submarine slope, NE Scotland. *Journal of the Geological Society, London*, **141**, 357–374, https://doi.org/10.1144/gsjgs.141.2.0357
Ragon, T., Nutz, A., Schuster, M., Ghienne, J.F., Ruffet, G. and Rubino, J.L. 2018 Evolution of the northern Turkana Depression (East African Rift System, Kenya) during the Cenozoic rifting: new insights from the Ekitale Basin (28–25.5 Ma). *Geological Journal*, **54**, 3468–3488, https://doi.org/10.1002/gj.3339
Ramsay, J. 1980. The crack–seal mechanism of rock deformation. *Nature*, **284**, 135–139, https://doi.org/10.1038/284135a0
Read, H.H. 1923. *The Geology of the Country Around Banff, Huntly and Turriff (Lower Banffshire and North-West Aberdeenshire) (Explanation of Sheets 86 and 96)*. Memoir of the Geological Survey, Scotland. HMSO, Edinburgh.
Roberts, A.M. and Holdsworth, R.E. 1999. Linking onshore and offshore structures: Mesozoic extension in the Scottish Highlands. *Journal of the Geological Society*, *London*, **156**, 1061–1064, https://doi.org/10.1144/gsjgs.156.6.1061
Roberts, A.M., Badley, M.E., Price, J.D. and Huck, I.W. 1990. The structural history of a transtensional basin: Inner Moray Firth, NE Scotland. *Journal of the Geological Society, London*, **147**, 87–103, https://doi.org/10.1144/gsjgs.147.1.0087
Roberts, N.M.W., Troy Rasbury, E., Parrish, R.R., Smith, C.J., Horstwood, M.S.A., and Condon, D.J. 2017. A calcite reference material for LA-ICP-MS U-Pb geochronology, *Geochemistry. Geophysics. Geosystems*, **18**, 2807–2814, https://doi.org/10.1002/2016GC006784
Roberts, N.M., Drost, K. *et al.* 2020*a*. Laser ablation inductively coupled plasma mass spectrometry (LA-ICP-MS) U–Pb carbonate geochronology: strategies, progress, and limitations. *Geochronology*, **2**, 33–61, https://doi.org/10.5194/gchron-2-33-2020
Roberts, N.M.W., Lee, J.K., Holdsworth, R.E., Jeans, C., Farrant, A.R. and Haslam, R. 2020*b*. Near-surface Palaeocene fluid flow, mineralisation and faulting at Flamborough Head, UK: new field observations and U–Pb calcite dating constraints. *Solid Earth*, **11**, 1931–1945, https://doi.org/10.5194/se-11-1931-2020
Rogers, D.A., Marshall, J.E.A. and Astin, T.R. 1989. Devonian and later movements on the Great Glen fault system, Scotland. *Journal of the Geological Society, London*, **146**, 369–372, https://doi.org/10.1144/gsjgs.146.3.0369
Rotevatn, A., Kristensen, T.B. *et al.* 2018. Structural inheritance and rapid rift-length establishment in a multiphase rift: the East Greenland rift system and its Caledonian orogenic ancestry. *Tectonics*, **37**, 1858–1875, https://doi.org/10.1029/2018TC005018
Sasvári, Á. and Baharev, A. 2014. SG2PS (structural geology to postscript converter) – a graphical solution for brittle structural data evaluation and paleostress calculation. *Computers & Geosciences*, **66**, 81–93, https://doi.org/10.1016/j.cageo.2013.12.010
Seranne, M. 1992. Devonian extensional tectonics versus Carboniferous inversion in the northern Orcadian basin. *Journal of the Geological Society, London*, **149**, 27–37, https://doi.org/10.1144/gsjgs.149.1.0027
Spang, J. 1972. Numerical method for dynamic analysis of calcite twin lamellae. *Geological Society of America Bulletin*, **84**, 134–150.
Steel, R. and Ryseth, A. 1990. The Triassic–early Jurassic succession in the northern North Sea: megasequence stratigraphy and intra-Triassic tectonics. *Geological Society, London, Special Publications*, **55**, 139–168, https://doi.org/10.1144/GSL.SP.1990.055.01.07
Stephenson, D. and Gould, D. 1995. *The Grampian Highlands*, 4th edn. British Regional Geology Series. HMSO, London.
Stewart, M., Strachan, R.A. and Holdsworth, R.E. 1999. Structure and early kinematic history of the Great Glen Fault Zone, Scotland. *Tectonics*, **18**, 326–342, https://doi.org/10.1029/1998TC900033
Stoker, M.S., Hitchen, K. and Graham, C.C. 1993. *The Geology of the Hebrides and West Shetland Shelves, and Adjacent Deep-Water Areas*, **2**. HMSO, London.
Sweet, I. 1985. The sedimentology of the Lower Old Red Sandstone near New Aberdour, Grampian Region. *Scottish Journal of Geology*, **21**, 239–259, https://doi.org/10.1144/sjg21030239
Tămaş, D.M., Tămaş, A., Barabasch, J., Rowan, M.G., Schleder, Z., Krézsek, C. and Urai, J.L. 2021. Low-angle shear within the exposed Mânzălești diapir, Romania: salt decapitation in the Eastern Carpathians fold-and-thrust belt. *Tectonics*, **40**, e2021TC006850, https://doi.org/10.1029/2021TC006850
Thomson, K. and Hillis, R.R. 1995. Tertiary structuration and erosion of the Inner Moray Firth. *Geological Society, London, Special Publications*, **90**, 249–269, https://doi.org/10.1144/GSL.SP.1995.090.01.16
Thomson, K. and Underhill, J.R. 1993. Controls on the development and evolution of structural styles in the Inner Moray Firth Basin. *Petroleum Geology Conference Series*, **4**, 1167–1178, https://doi.org/10.1144/0041167
Tomasso, M., Underhill, J.R., Hodgkinson, R.A. and Young, M.J. 2008. Structural styles and depositional architecture in the Triassic of the Ninian and Alwyn North fields: implications for basin development and prospectivity in the Northern North Sea. *Marine and Petroleum Geology*, **25**, 588–605, https://doi.org/10.1016/j.marpetgeo.2007.11.007
Trewin, N.H. 1987. Pennan, unconformity within the Old Red Sandstone, Excursion 8. *In*: Trewin, N.H.T., Kneller, B.C. and Gillen, C. (eds) *Excursion Guide to the Geology of the Aberdeen Area*. Scottish Academic Press, Edinburgh, 127–130.
Trewin, N. and Hurst, A. 2009. *Excursion Guide to the Geology of East Sutherland and Caithness*, 2nd edn. Dunedin Academic Press, Edinburgh.
Trewin, N.H.T., Andrews, S.D. and Kneller, B.C. 1987. The Lower Old Red Sandstone of New Aberdour. *In*: Trewin, N.H.T., Kneller, B.C. and Gillen, C. (eds), *Excursion Guide to the Geology of the Aberdeen Area*, Scottish Academic Press, Edinburgh.
Underhill, J.R. 1991. Implications of Mesozoic–recent basin development in the western Inner Moray Firth, UK. *Marine and Petroleum Geology*, **8**, 359–369, https://doi.org/10.1016/0264-8172(91)90089-J
Underhill, J.R. and Brodie, J.A. 1993. Structural geology of Easter Ross, Scotland: implications for movement on the Great Glen fault zone. *Journal of the Geological Society, London*, **150**, 515–527, https://doi.org/10.1144/gsjgs.150.3.0515
Underhill, J.R. and Partington, M.A. 1993. Jurassic thermal doming and deflation: the sequence stratigraphic evidence. *In*: Parker, J.R. (ed.) Petroleum

Geology of North-West Europe: Proceedings of the 4th Conference. Geological Society, London, 337–345, https://doi.org/10.1144/0040337

Vermeesch, P. 2018. IsoplotR: a free and open toolbox for geochronology. *Geoscience Frontiers*, **9**, 1479–1493, https://doi.org/10.1016/j.gsf.2018.04.001

Wallace, R.E. 1951. Geometry of shearing stress and relation to faulting. *Journal of Geology*, **59**, 118–130.

Watts, L.M., Holdsworth, R.E., Sleight, J.A., Strachan, R.A. and Smith, S.A.F. 2007. The movement history and fault rock evolution of a reactivated crustal-scale strike-slip fault: the Walls Boundary Fault Zone, Shetland. *Journal of the Geological Society, London*, **164**, 1037–1058, https://doi.org/10.1144/0016-76492006-156

Weismüller, C., Urai, J.L., Kettermann, M., von Hagke, C. and Reicherter, K. 2019. Structure of massively dilatant faults in Iceland: lessons learned from high-resolution unmanned aerial vehicle data. *Solid Earth*, **10**, 1757–1784, https://doi.org/10.5194/se-10-1757-2019

Wilson, R.W., McCaffrey, K.J.W., Holdsworth, R.E., Imber, J., Jones, R.R., Welbon, A.I.F. and Roberts, D. 2006. Complex fault patterns, transtension and structural segmentation of the Lofoten Ridge, Norwegian margin: using digital mapping to link onshore and offshore geology. *Tectonics*, **25**, https://doi.org/10.1029/2005TC001895

Wilson, R.W., Holdsworth, R.E., Wild, L.E., McCaffrey, K.J.W., England, R.W., Imber, J. and Strachan, R.A. 2010. Basement influenced rifting and basin development: a reappraisal of post-Caledonian faulting patterns from the North Coast Transfer Zone, Scotland. *Geological Society, London, Special Publications*, **335**, 795–826, https://doi.org/10.1144/SP335.32

Woodcock, N.H. and Strachan, R.A. 2012. *Geological History of Britain and Ireland*. Wiley, Chichester.

Zanella, E. and Coward, M.P. 2003. Structural framework. *In*: Evans, D., Graham, C., Armour, A. and Bathurst, P. (eds) *The Millennium Atlas: Petroleum Geology of the Central and Northern North Sea*. Geological Society, London, 45–59.

Zanella, E., Coward, M.P. and McGrandle, A. 2003. Crustal structure. *In*: Evans, D., Graham, C., Armour, A. and Bathurst, P. (eds) *The Millennium Atlas: Petroleum Geology of the Central and Northern North Sea*. Geological Society, London, 35–42.